THESIS FOR THE DEGREE OF LICENTIATE OF ENGINEERING

Decreased furnace wall corrosion in fluidised bed boilers

The influence of fuel lead content and sewage sludge additive

Annika Talus

Department of Chemistry and Chemical Engineering

CHALMERS UNIVERSITY OF TECHNOLOGY

Gothenburg, Sweden 2016

Decreased furnace wall corrosion in fluidised bed boilers

The influence of fuel lead content and sewage sludge additive

Annika Talus

Technical report no 2016:17
ISSN: 1652-943X

Department of Chemistry and Chemical Engineering

Chalmers University of Technology
SE-412 96 Gothenburg
Sweden
Telephone + 46 (0)31-772 1000

annika.talus@chalmers.se
annika.talus@swerea.se

Cover: SEM image illustrating corrosion of 16Mo3 exposed when combusting wood fuel with a lead concentration of 1000 mg/kg fuel, (see subchapter 6.1.2 for more details).

Chalmers Reproservice
Gothenburg, Sweden 2016

Abstract

Usage of used-wood fuel in the power industry has resulted in increased corrosion problems for metallic materials in the boilers, most probably due to relatively high amounts of chlorine, alkali metals and heavy metals present in the fuel.

In this investigation, laboratory exposures were performed in order to study the influence of lead content in a wood-based fuel on the corrosion of selected materials. Field exposures were also performed to investigate whether co-firing sewage sludge with used-wood fuel could decrease the corrosion of materials in a boiler. Temperatures studied were 350 °C and 400 °C and the exposures were performed at furnace wall position for 8-14 h.

The findings showed increased corrosion of the low-alloyed steel 16Mo3 when increasing the lead content in the fuel. At 350 °C, the corrosion was minor but at 400 °C it was considered severe. The explanation for the corrosion at 400 °C was proposed to be a reaction between lead oxide and/or metallic lead, present in the deposit, with iron chloride, formed in the initial corrosion process, resulting in the formation of iron oxide and lead chloride. The presence of lead chloride in the deposit together with, in this case, potassium chloride, results in a very corrosive deposit due to formation of a low melting temperature salt mixture, traces of which were found in the oxide of the corroded samples. For the other tested materials negligible corrosion was observed.

It was found that co-firing sewage sludge with a used-wood fuel decreased the corrosion for all tested materials.

Keywords: Furnace wall corrosion, used-wood, demolition-wood, sewage sludge, chlorine-induced corrosion, alkali chloride, lead oxychloride, lead oxide, salt melt.

List of publications

The thesis is based on the following appended papers/publications:

Paper I
Y. Alipour, A. Talus, P. Henderson, and R. Norling
The effect of co-firing sewage sludge with used wood on the corrosion of an FeCrAl alloy and a nickel-based alloy in the furnace region
Fuel Processing Technology, **138**, 805 (2015).

Paper II
A. Talus, Y. Alipour, R. Norling and P. Henderson
Initial corrosion of 16Mo3 and 310S when exposed in a used fired boiler with and without sewage sludge additions
Materials and Corrosion, **67**, 683 (2016)

Paper III
A. Talus, R. Norling, Leyla Wickström and A. Hjörnhede
Effect of lead content in used wood fuel on furnace wall corrosion of 16Mo3, 304L and Alloy 625
Accepted for publication in *Oxidation of metals*, (2016)

Statement of author's contribution

In Paper I I was involved in the evaluation of samples after exposure and main responsible for evaluation of GD-OES-results with assistance of experts at Swerea KIMAB. I also assisted in writing the paper.

In Paper II I was the main author of the paper. I performed the main part of the evaluation of samples after exposure, including the SEM of cross sections, the XRD of surfaces and the FIB cross sectioning with assistance from an instrument driver. The evaluation of GD-OES-results was performed by me with assistance from experts at Swerea KIMAB.

In Paper III I was the main author of the paper. I performed the main part of the evaluation of the samples after exposure, including sample preparation, SEM and XRD evaluations of surfaces and cross sections.

Related work

The following work has not been included in this thesis but is related to the research area.

K. Yuan, R. L. Peng, X-H. Li, A. Talus, S. Johansson and Y-D. Wang
Hot corrosion of MCrAlY coatings in sulphate and SO_2 environment at 900 °C: Is SO_2 necessarily bad?
Surface and Coatings Technology, **261**, 41, (2015).

A. Talus, R. Norling, and P. Henderson
Influence of ammonium sulphate additive on superheater corrosion at increased steam temperature during combustion of recycled wood
10th Liège Conference on Materials for Advanced Power Engineering, Liege, (2014).

List of acronyms

BSE	Back scattered electrons
BFB	Bubbling fluidised bed
CFB	Circulating fluidised bed
CHP	Combined heat and power
EDS	Energy dispersive spectrometry
FIB	Focused ion beam
GD-OES	Glow discharged optical emission spectroscopy
SE	Secondary electrons
SEM	Scanning electron microscope
XRD	X-ray diffraction

Table of Contents

1 Introduction

The climate change the world is facing is of concern for both individuals and industry. One way to combat this change is to decrease dependency on fossil fuels. In the power industry, coal and oil are major fuel sources and have been so for a long duration of time. However, in Sweden, the use of more environmentally friendly fuels has increased during the last decades. Different wood fuels can be included in this category, and, for instance, used wood (also known as recycled, waste and demolition wood) is a fuel that is commonly used.

Changing the fuel source in a boiler is, however, not done without introducing new challenges. The metallic materials in the boilers are dimensioned for coal and oil combustion, and introducing new fuels has shown to greatly affect the life expectancy of the materials mainly due to greater problems with corrosion [1, 2]. The corrosion problems present when firing wood fuels have been shown to be related to the large amount of corrosive species released to the flue gas during combustion. In particular, the corrosion caused by hydrogen chloride and alkali chlorides is a problem that has been widely studied [3-8]. When firing used-wood fuels, the corrosion problem is also believed to be attributed to the presence of heavy metals, such as lead and zinc, in the fuel. Important sources of these elements are paint remains (Pb) and galvanised nails or screws (Zn) [9-11]. The presence of these elements in deposits at the surface of boiler materials has been demonstrated [2, 12], however, how they affect the materials is less known.

Due to the corrosion accelerating properties of used-wood fuels, attempts are being made to counteract these problems. Injection or co-combustion of an additive is a possible method to use. The additives contain species that are to capture the corrosive species in the flue gas and give rise to a less corrosive environment in the boiler. This has been shown to work well at the superheater position in the boiler where a decrease in corrosion has been found when co-firing an additive rich in sulphur [13-16].

The environment in boilers is, however, very complex and varies greatly depending on location. For this reason, different corrosion problems can occur depending on

temperature, flue gas composition and material selection throughout the boiler. Thus, in order to solve corrosion problems, one single solution is often not enough for a boiler as a whole. Instead, different solutions may be needed at different locations in the boiler.

1.1 Aim of the thesis

This thesis follows two lines both of which aim to increase knowledge about the relation between fuel composition and corrosion problems that occur at the furnace wall position in a used-wood-fired boiler. At this position, the combustion conditions are expected to primarily be reducing. The research investigates the influence of lead content in a wood fuel on the corrosion of selected materials. In addition, the influence of co-firing with the additive municipal sewage sludge is evaluated with respect to how it may reduce corrosion.

2 Oxidation

Metallic materials are, in general, thermodynamically unstable when exposed to environments where oxygen is present. This means that a reaction between the metallic material and oxygen in the environment will take place and form a metal oxide on the metal substrate according to Equation (1) .

$$xM(s) + y/2\ O_2(g) \rightarrow M_xO_y(s) \quad (1)$$

2.1 Thermodynamics

The oxidation of a metallic material is dependent on how favourable the oxidised state is from an energy point of view. The driving force for a reaction is a function of temperature, T, and the equilibrium constant, K, for the reaction and is described by the Gibbs free energy, G, according to Equation (2) where R is the ideal gas constant. The equilibrium constant is expressed by using the activity, a, of the solid compounds and/or partial pressures, p, of the gaseous compounds present as reactants and products in a reaction according to Equation (3) [17].

$$\Delta G^0 = -RT \ln K \quad (2)$$

$$K = (a_{MxOy}/(a_M^x * p_{O2}^{y/2})) \quad (3)$$

A negative value indicates that the oxidised state is a more favourable state than the non-oxidised state. The more negative value a reaction has the more likely it is to occur. A positive value means that the reaction does not occur spontaneously and energy is needed for the reaction. In an Ellingham diagram, (see Figure 1), the Gibbs free energy is plotted as a function of temperature illustrating the ability of different materials to form oxides. The lower the position in this diagram, the more stable the oxide of a metal is. Since the oxidation of a metal is also dependent on the oxygen partial pressure (pO_2) in the atmosphere, a scale bar with different oxygen partial pressures is present in the diagram. This can be used to determine if an oxide is stable or not at a certain oxygen partial pressure [18].

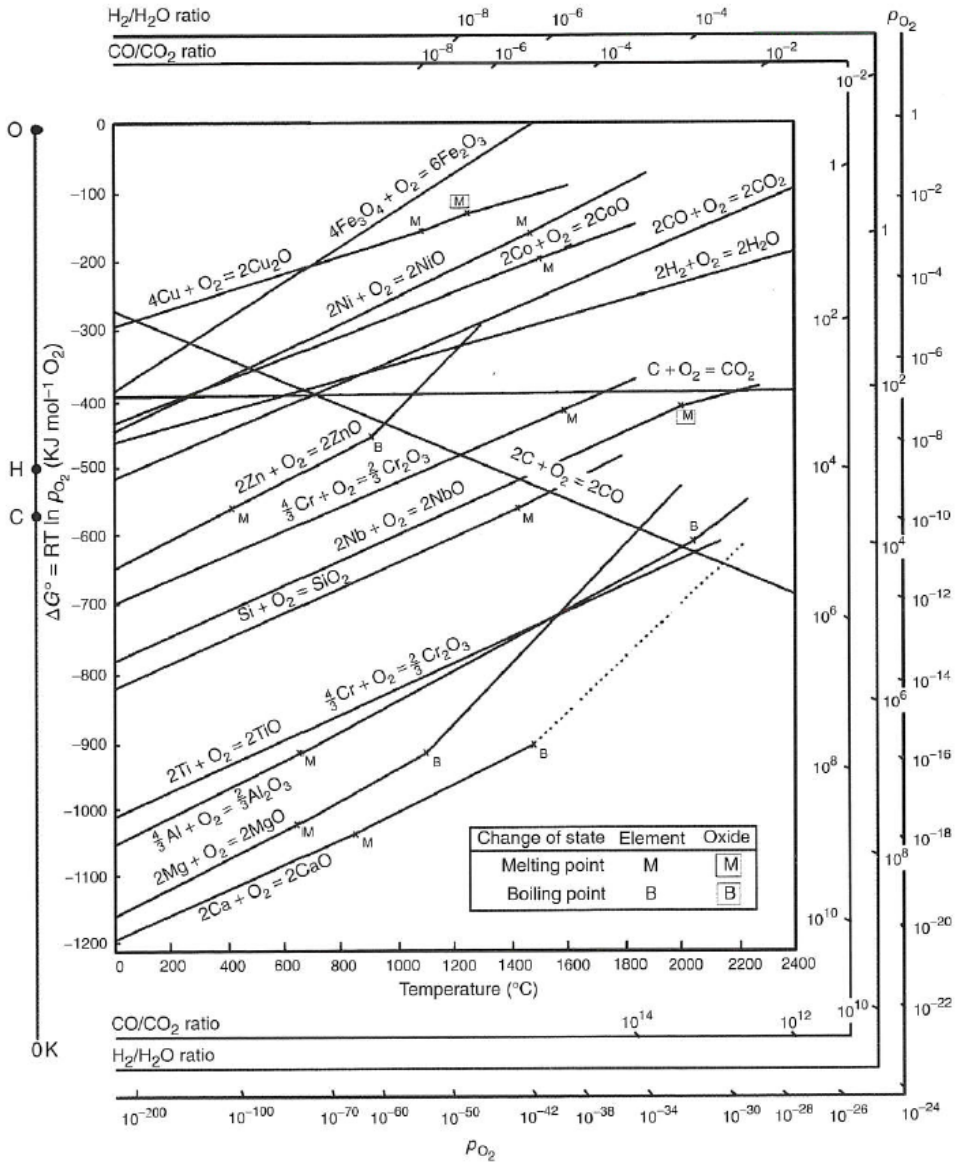

Figure 1. Ellingham diagram describing the driving force for oxidation of metals depending on temperature [18].

2.2 Initial oxide formation

Oxide formation starts when molecules containing oxygen like O_2 or H_2O are adsorbed on the metal surface and dissociated into oxygen atoms. The oxygen atoms become charged (O^{2-}) due to the attraction of electrons, and, in a subsequent step, the oxygen reacts with the metallic material, and nucleation of metal oxide occurs on the metal substrate. The growth of the oxide nucleates result in the formation of a thin oxide layer along the surface of the material.

When this oxide layer has formed, oxygen ions need to be transported inwards through the already formed oxide, or metal ions need to be transported outwards to further oxidise the metal [19]. An illustration of the initial oxidation process is provided in Figure 2.

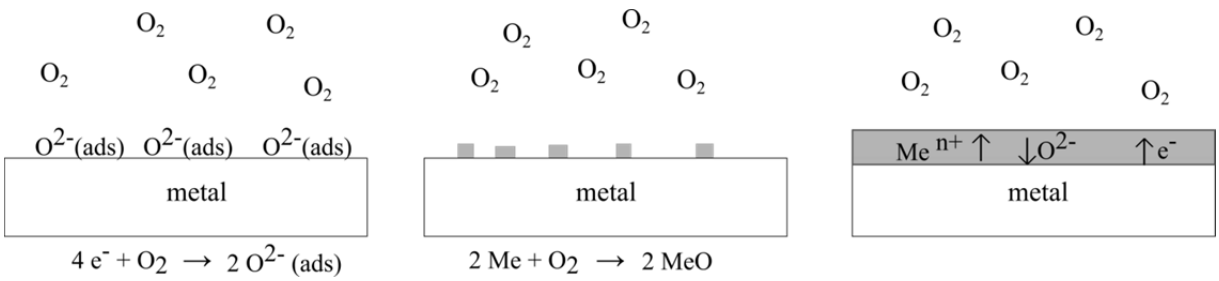

Figure 2. Illustration of initial oxide formation on a metal surface exposed to oxygen.

2.3 Kinetics

When an oxide layer has formed on the metal substrate, the rate limiting step becomes the transport of ions through the oxide layer in order for oxygen to meet the metal. The propagation of oxide growth can be described with different rate equations; linear, parabolic and logarithmic, (see Figure 3).

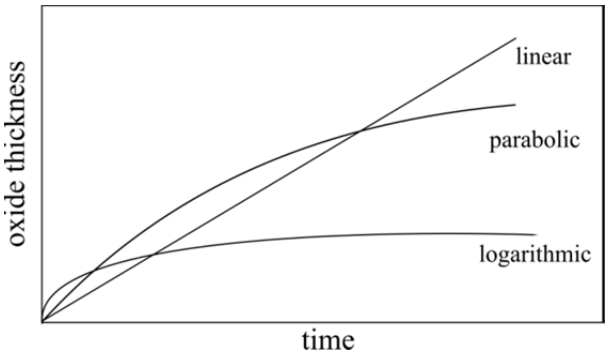

Figure 3. Oxidation kinetics for linear, parabolic and logarithmic rate equations.

In order to be protective, a metal oxide must act as a good barrier to oxygen and metal diffusion. These properties vary depending on metal oxide and also depending on temperature and atmosphere where the metal is used. A linear growth rate of the oxide can be adapted in the beginning of the oxidation when the rate limiting step is not the

diffusion of atoms through an oxide scale [18]. When the diffusion of atoms becomes the rate controlling step, the oxidation often proceeds in a parabolic manner. At lower temperatures (300-400 °C), the oxidation is often described as logarithmic, with an initially rapid oxidation that transcend into a low oxidation rate [19].

2.4 Metal oxides

2.4.1 Iron oxides

Depending on temperature and oxygen access, several iron oxides can be formed when iron is oxidised (wüstite FeO, hematite Fe_2O_3 and magnetite Fe_3O_4). Due to its ability to form several oxides, iron forms a multi-layered oxide structure in the order of FeO, Fe_3O_4 and Fe_2O_3 (from the metal substrate and out) if the temperature is sufficiently high [18]. Of the three oxides, Fe_2O_3 is the most protective due to its crystal structure with low defect concentration. Wüstite does not form until over 570 °C and is the least protective oxide of the three due to its non-stoichiometric structure, which allows fast ion diffusion and, consequently, fast oxide growth. Magnetite has a spinel structure and behaves less protectively than Fe_2O_3, however, compared to FeO it is more stoichiometric and, thus, considered more protective [19].

2.4.2 Chromium oxides

Chromium forms only one oxide at higher temperatures, chromia Cr_2O_3. This oxide is considered to be a protective oxide since it has slow solid state diffusion properties. However, at temperatures over 1000 °C chromia evaporate and are, thus, not suitable at high temperatures [19].

2.4.3 Aluminium oxides

Depending on temperature, aluminium forms different crystal structures of its oxide Al_2O_3. The most protective aluminium oxide is α-Al_2O_3, corundum, which has a slow growth rate due to its high stoichiometric structure [19].

3 Thermal power production

Power production through combustion implies that a fuel is fired to generate electricity. The fuel combustion takes place in a furnace and the walls of the furnace consist of metal tubes that contain flowing water. This water is heated when combustion takes place, and an overheated steam is produced that runs turbines that generate electric power. In Sweden, it is common that power plants are used for combined heat and power production (CHP). This means that the water that has been heated in order to generate electricity is also used for district heating.

3.1 Combustion

During combustion, several reactions take place that consume oxygen, (see common reactions in Equations (4)-(5)). If the combustion is complete, the commonly produced gaseous species will be water and carbon dioxide. An incomplete combustion has residuals of carbon monoxide and hydrogen in the flue gas and is often a result of that the temperature has been too low during combustion.

$$H_2(g) + ½\ O_2(g) \rightarrow H_2O(g) \quad (4)$$

$$C(s) + O_2(g) \rightarrow CO_2(g) \quad (5)$$

In order to reach complete combustion, the addition of oxygen is often needed in the boilers. This is achieved with the use of several air inlets at different positions in the boiler. There are several different designs of boilers. In this thesis, bubbling fluidised bed boilers were used in all tests and are further described in the following subchapter.

3.1.1 Fluidised bed boilers

In a fluidised bed boiler, the fuel is combusted in a fluidised bed that often consists of sand particles. Air flows from the bottom of the boiler (primary air) and this results in the expansion of the sand particles, which gives rise to the fluidised bed. Depending on

the air flow, the bed can be either bubbling or circulating. In a bubbling fluidised bed boiler (BFB), the air flow is controlled in a way that the sand particles remain in the bed, (see illustration in Figure 4). In the circulating fluidised bed boiler (CFB), the flow is high enough for the sand particles to follow the flue gas, and a cyclone is present to separate the sand particles from the flue gas before entering the superheater area. After the sand particles have been separated from the flue gas they are recirculated to the bed.

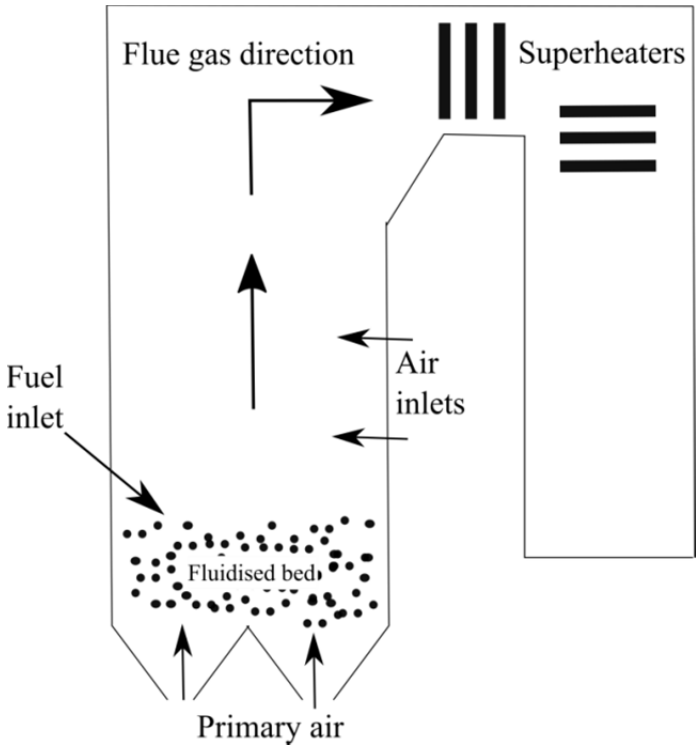

Figure 4. Schematic illustration of a bubbling fluidised bed boiler.

The bed temperature in a BFB is often in the range of 800-900 °C in order to achieve complete combustion [20]. These boilers have good flexibility regarding fuel type due to evenly distributed temperature and large thermal mass in the bed. When the fuel is fed to the hot bed together with oxygen, it ignites and the firing process starts. As mentioned above, primary air flows from the bottom of the boiler, and oxygen is consumed in the firing process. Air is also added in two later steps (secondary and tertiary air) in order to ensure that full combustion is achieved. For this reason, oxygen partial pressure will vary throughout the boiler.

3.1.2 Fuel properties and consequences of fuel change

Elemental composition varies with fuel. This is an important factor when changing the fuel from coal and oil to other more environmentally friendly fuels. The difference in chemical composition between coal and used wood is illustrated in Table 1. For instance, a higher concentration of chlorine and heavy metals are present in used-wood fuel at the same time as this fuel often has a lower sulphur content. This will consequently result in differences in flue gas composition, which will have an influence on the corrosion of metallic materials in the boiler.

Table 1.Energy content of selected fuels.

Fuel	Elemental analysis [wt%, dry, ash free base]					[wt% dry base]		
	C	H	O	S	N	Cl	Zn	Pb
Coal [21]	78.2	5.2	13.6	1.7	1.3	0.03	-	-
Used wood [9]	52	6	41	0.07	0.84	0.05	0.5	0.05

3.1.3 Flue gas and deposit composition

The combustion process results in a flue gas that generally contains carbon dioxide and water. Depending on fuel composition, other compounds can be present in the flue gas as well. For fuels with a high sulphur content, like coal, sulphur dioxide is expected to be present in the flue gas. Changing to a used-wood fuel will result in an increase in several elements in the fuel. The increase of chlorine and heavy metals is presented in Table 1, but alkali metals (potassium and sodium) are also known to be present in these fuels. This will result in an increase in hydrochloric acid (HCl), alkali metals (KCl, NaCl) and heavy metals in the flue gas.

When the flue gas meets a surface that is cooler than the gas, condensation of different species can take place on the metal surface. Both flue gas temperatures and metal temperatures vary throughout the boiler and will result in differences in condensed species [22-24]. At the furnace wall position, the flue gas temperature is often higher than the flue gas temperature at superheater position. The metal temperature is on the other hand lower at the furnace wall position than at the superheater position. Also, the environment is usually described as reducing in the

lower part of the furnace since oxygen is consumed in the firing process. In contrast, at the position of the lower superheaters, the environment is considered to be oxidising since more oxygen is present there as a result of the tertiary air inlet present in the upper part of the furnace. However, since combustion is not always ideal, fluctuations will most probably occur between reducing and oxidising conditions at the furnace walls. All these parameters influence the condensation of species from flue gas. Depending on the species that are condensed on the metal tube surfaces, the deposit becomes more or less corrosive.

3.2 Corrosion problems when burning used-wood fuels

At high temperatures, most reactions are faster than at lower temperatures, including the oxidation of metals. As explained in the introduction, the power industry faces new challenges when it changes fuel, for instance, to used-wood fuel. This is partly due to the fact that the atmosphere in the boilers becomes more aggressive with an increase in the amount of hydrochloric acid and alkali chlorides in the flue gas. Also heavy metals like Zn and Pb have been shown to be present in deposits on samples exposed to used-wood fuels [2, 12, 25].

3.2.1 Chlorine-induced corrosion

It is well known today that chlorine can have a negative influence on the corrosion behaviour of metallic materials. The mechanism at high temperatures is debated, and there is more than one suggestion for how chlorine contributes to corrosion.

One commonly referred mechanism is active oxidation [26] in which chlorine is suggested to penetrate the metal oxide as $Cl_2(g)$ and react with the metal according to Reaction (6). The product becomes a metal chloride that is stable at the low oxygen partial pressure, pO_2, present below the oxide. The metal chloride has, however, a high vapour pressure in the environment that prevails below the oxide scale and will evaporate towards the sample surface. On the way to the surface, the oxygen partial pressure increases and the metal chloride becomes unstable, reacts with oxygen and

forms metal oxide and chlorine gas, (see Reaction (7)). This chlorine can, once again, penetrate the oxide scale and form metal chlorides. Also HCl has been suggested to be the corrosive species that is reacting with the iron instead of Cl_2 [27]. This suggestion is based on thermodynamic calculations that indicate that HCl is present in the gas phase and is more stable than Cl_2 in H_2O-rich atmospheres.

$$Cl_2(g) + Fe(s) \rightarrow FeCl_2(s) \quad (6)$$

$$FeCl_2(g) + \tfrac{3}{4}\, O_2(g) \rightarrow \tfrac{1}{2}\, Fe_2O_3(s) + Cl_2(g) \quad (7)$$

Another theory is that HCl reduces oxygen to water vapour and chlorine ions at the sample surface. According to this theory, the chlorine ions would then be transported inwards towards the metal/oxide interface simultaneously as metal ions are transported outwards, and, when they meet metal chlorides are formed [3].

3.2.2 Chromium oxide hydroxide evaporation

Chromium oxide is considered to be a protective oxide at higher temperatures (<1000 °C). However, by introducing water vapour into the atmosphere, chromium oxide has been shown to be unstable due to the formation of chromium oxide hydroxide, which is volatile and easily evaporates, (see Equation (8)). This has been shown to happen at temperatures as low as 600 °C [28].

$$\tfrac{1}{2}\, Cr_2O_3(s) + H_2O(g) + \tfrac{3}{4}\, O_2(g) \rightarrow CrO_2(OH)_2(g) \quad (8)$$

3.2.3 Alkali-induced corrosion

There are studies that show that not only is the chlorine ion aggressive to metallic materials but also is the alkali ion. It has been shown that when a material with a protective chromium oxide is exposed to potassium chloride at 600 °C, potassium chromates are formed (Equation (9)) [29]. This reaction results in a chromium depleted oxide which is less protective than the original chromium oxide and increase the risk for corrosion. In this example, (Equation (9)), the effect of potassium chloride

is illustrated, however, studies have shown that several different alkali compounds, such as potassium carbonate and sodium chloride, can result in chromate formation as well [8, 30]. Chromates have also been found in tests performed at 400 °C [5].

$$\tfrac{1}{2}\ Cr_2O_3(s) + 2\ KCl(s) + \tfrac{3}{4}\ O_2(g) + H_2O(g) \rightarrow K_2CrO_4(s) + 2\ HCl(g) \qquad (9)$$

For low-alloyed steel no chromate formation is expected, however, increased corrosion has been observed for this type of material when exposed to small amounts of KCl [31]. The effect of potassium chloride on corrosion was observed when it was located on a metal substrate in the presence of water vapour (20%) and oxygen (5%). It was suggested in the study [31] that the formation of potassium hydroxide releases chlorine ions, (see Equation (10)), which then further act as a catalyst for chlorine-induced corrosion while the high vapour pressure of potassium hydroxide results in the vaporisation of this compound.

$$2KCl(s) + \tfrac{1}{2}O_2(g) + H_2O(g) + 2e^- \rightarrow 2KOH(ads) + 2\ Cl^-(ads) \qquad (10)$$

Deposits with a high amount of alkali chlorides, thus, increase the risk for corrosion of both low-alloyed steels and chromia-forming alloys.

3.2.4 Corrosion below salt melts

Depending on the metal temperature at different locations in a boiler, parts of a deposit could melt due to its content of low melting salt mixtures. In Table 2, melting points for common salts and the salt mixtures that may be present in such deposits are listed [32, 33]. The presence of a salt melt facilitates the transport of ions through the deposit, and corrosion processes are often accelerated. Several studies have shown the negative effect of a salt melt present on a metal substrate [34-38].

Table 2. Melting points for salts and lowest eutectic temperatures for salt mixtures.

Salt	Melting point °C [32]	Salt mixture	Lowest eutectic temperature °C [33]
NaCl	801	$NaCl – PbCl_2$	410
		$NaCl – ZnCl_2$	262
KCl	771	$KCl – PbCl_2$	411
		$KCl – ZnCl_2$	230
$FeCl_2$	677	$FeCl_2 –PbCl_2$	421
		$FeCl_2 – NaCl$	370
		$FeCl_2 – KCl$	355
		$FeCl_2 – ZnCl_2$	300
$PbCl_2$	498		
$ZnCl_2$	318		

The lowest eutectic temperature for a salt mixture decreases when heavy metals are present in the salt, as can be seen in Table 2. Thus, the involvement of lead and /or zinc in a deposit will dramatically increase the risk of corrosion due to the possible formation of salt melts.

3.3 Use of additives to decrease corrosion

In order to decrease corrosion problems in the power plants, co-firing of different additives, which often contain sulphur, has been shown to be effective [13-16]. This has shown to be effective in the areas of the boiler where the oxygen level is relatively high and the sulphur-containing additive converts the corrosive alkali metals into less corrosive alkali sulphates. An interesting additive not so commonly used is municipal sewage sludge. This additive contains a high amount of compounds that have been suggested to act as alkali-capture substances [39] and could, thus, possibly decrease corrosion when co-fired with used-wood fuels. Some studies have shown the positive effect of this additive on decreasing superheater corrosion [40-44].

4 Analytical techniques

In order to get the full picture of what happens during an exposure, it is very useful, if not necessary, to combine different analysis techniques when evaluating exposed samples. Several analytical techniques have been used in this thesis and are described in the following subchapters.

4.1 Scanning electron microscopy (SEM)

Scanning electron microscopy (SEM) has been used frequently in the evaluation of samples in this thesis in order to study cross-section appearance in detail and also to gather information about chemical composition at various places in the cross sections and of the deposit on the surface of the samples.

This technique uses electrons to produce an image. A focused electron beam scans a specimen, and when electrons hit the sample, they interact with the atoms in the sample and send different signals back. When the primary electrons hit the specimen, a certain volume is penetrated, and this is called the interaction volume. From this area, different signals are activated. Commonly used signals for imaging and analysis are secondary electrons (SE), backscattered electrons (BSE) and X-rays. These signals originate from different depths within the specimen and are often used in combination in order to get the most out of an analysis. In Figure 5, an illustration of the interaction volume is presented together with the depth from which the different signals come.

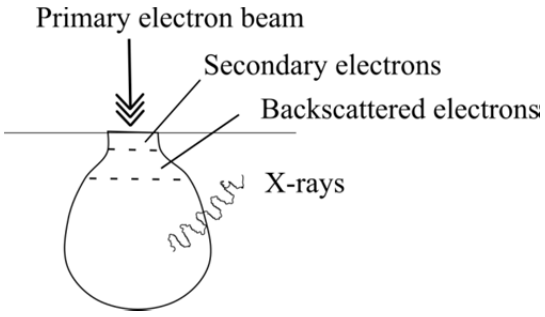

Figure 5. Illustration of interaction volume.

A secondary electron is an electron that has been affected by a primary electron and from this interaction, gained a small amount of energy. Due to its low energy <50eV the electrons escapes the sample from areas close to the sample surface. These electrons are useful for topographical studies of a sample.

A backscattered electron is a primary electron that leaves the sample surface before giving up all its energy. When escaping the sample surface, these electrons often have a large fraction of their incident energy left. These electrons give elemental contrast of a sample. More electrons are backscattered the higher the atom number of an element is. An element with higher atom number will, thus, appear lighter compared to an element with a lower atom number.

When the primary electrons interact with a specimen, atoms in the specimen are affected. Electrons in the electron shell of an atom will be knocked out, and this results in a high energy state of the atom. In order to fill the gap in the atom, an electron from an outer shell in the atom can replace the knocked out electron, and when this happens, X-ray signals that originate in the relaxation of the atom are formed. The energy of these signals is the difference between the high energy state of the atom and the energy state of the atom after relaxation. This energy is characteristic for a particular atom and, thus, this signal can tell the chemical composition of a specimen. By using an energy dispersive spectrometer (EDS), the X-ray spectrum achieved from the specimen can be measured and quantified. The energy of the X-rays also represents a certain wavelength. Thus, also the wavelengths can be used in order to obtain chemical information about the sample. For this purpose, a wavelength dispersive spectrometer (WDS) was used in this research [45].

Two instruments were used in this study; JEOL 7000 SEM and JEOL 7001 SEM, both equipped with an Oxford Inca detector for chemical analysis.

4.1.1 Focused ion beam (FIB)

The preparation of a cross section for analysis in SEM often requires some exposure to air and humidity. Even though dry sample preparation is an option when a sample is sensitive to humidity, some corrosion products are so sensitive to humidity that the

humidity in the air causes a reaction before the sample is put under vacuum in the SEM. In order to avoid this, the focused ion beam (FIB) technique can be used. This is a technique that performs ion milling of the sample under vacuum. In this work, two instruments were used; a FEI Versa 3D FIB/SEM and a FEI Quanta 3D FIB/SEM.

In order to obtain a chemical analysis without any exposure to air humidity, some kind of chemical analysis equipment, like EDS or WDS, must be installed in the microscope as well. The FEI Quanta 3D instrument used in this work is equipped with an energy dispersive spectrometer connected to an INCA system from Oxford Instruments.

4.2 X-ray diffraction (XRD)

In order to study crystalline phases in the deposits on tested samples, X-ray diffraction (XRD) was used. This gives information about what has formed or has been deposited on the samples during an exposure.

The technique is based on irradiating a sample with X-rays that are diffracted in a certain pattern, depending on the crystalline phase that is irradiated. The diffracted X-rays interfere destructively or constructively, and it is the latter that is detected as a signal.

The difference in path length of two incident waves of radiation, scattering from different parallel lattice planes, is a function of lattice plane distance (d_{hkl}) and incident angle (θ) relative to the lattice plane. By varying the incident angle, it can be determined for which incident angles that constructive interference occurs, i.e. when the difference in path length of two incident waves are equal to an integer multiple of the weave length λ, and the scattered waves remain in phase. The relationship for constructive interference is described by Bragg's Law, (see Equation (11). A crystal structure of a given material can thus be related to the X-ray diffraction patterns obtained by relating the lattice plane distance (d_{hkl}) to the miller indices [46].

Braggs law: $\lambda = 2d \sin \theta$ (11)

For the samples examined in this thesis, D8 equipment (Bruker AXS) with a Cu Kα X-ray source was used. A Goebbel mirror for parallel beam arrangement was used, and a SolX (Bruker) energy dispersive detector was used to detect diffracted X-rays. The settings of the X-ray source and detector were Bragg Brentano θ-θ arrangement, meaning that both the X-ray source and the detector were in motion and the sample was fixed, according to the illustration in Figure 6.

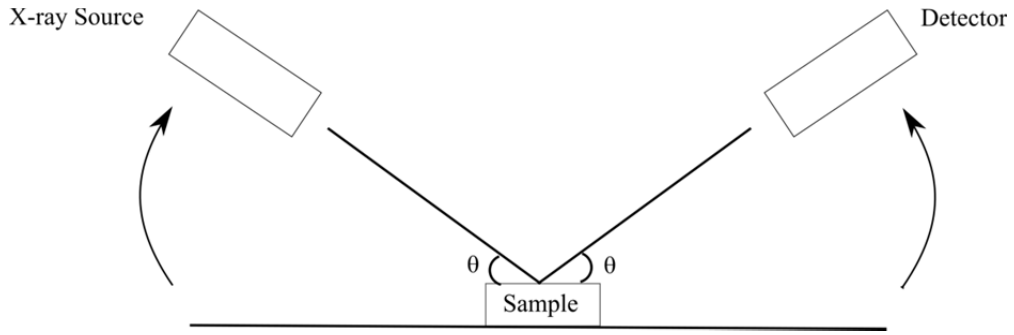

Figure 6. Illustration of X-ray diffraction equipment with "Bragg-Brentano θ-θ"-arrangement.

4.3 Glow discharged optical emission spectroscopy (GD-OES)

To study the chemical profile from the top of a deposit towards the oxide/metal interface and into the metal, glow discharged optical emission spectroscopy (GD-OES) can be used. This technique gives a relatively fast response to the chemical profile through the deposit, and, in general, very little sample preparation is necessary.

The specimen is bombarded with argon ions on a circular area of 2-4 mm in diameter. When the argon atoms hit the sample surface, the atoms on the specimen surface are sputtered away layer by layer. The characteristic light emission from this process is analysed with an optical emission spectrometer and the depth profile of the chemical concentrations in the deposit and oxide are, thus, obtained.

The instrument used in this thesis was a Leco GDS 850A. The sputtering was performed with an Ar-plasma at a potential of 700V and a current of 20 mA.

5 Experimental

In order to understand how different factors influence the high temperature corrosion of different materials, both fundamental research in the laboratory and applied tests in the field are often necessary. Both of these approaches were used in this work.

5.1 Materials

Findings for four material groups are presented in this thesis; low-alloyed steels, stainless steels, nickel-base alloys and FeCrAl alloys. The low-alloyed steel 16Mo3 is a material typically used in water wall tubes at the furnace wall position today due to its good mechanical properties. When used-wood fuel is burned, the corrosion behaviour of this material has, though, shown to be poor [47]. The material is used as a reference here, and, due to its often fast corrosion response, it was a good material for the initial corrosion studies performed in this thesis.

Due to the poor corrosion behaviour of 16Mo3 when exposed to a corrosive fuel, the water wall tubes are often coated with a material that has better corrosion properties. For this purpose, nickel-base alloys are commonly used at the furnace wall position. In order to study the corrosion behaviour also for such a material, the nickel-base Alloy 625 was included in this thesis. Furthermore, two types of stainless steels and the FeCrAl alloy Kanthal APMT were studied in order to test a range of materials. The FeCrAl alloy was pre-oxidised before exposure for 8 h at 1050 °C to produce a 1 µm thick alumina layer on the sample surface. The chemical compositions of the materials exposed in the different tests are presented in Table 3.

Table 3. Chemical composition of tested materials in wt%.

Alloy	C	Fe	Cr	Ni	Mo	Nb	Mn	Si	Al	Cu	N	Ti
16Mo3	0.148	Bal.	0.16	0.06	0.27	0.003	0.69	0.22	0.009	0.10	0.006	0.001
304L	0.020	Bal.	18.2	8.4	0.38	0.022	1.14	0.45	0.006	0.50	0.076	0.004
310S	0.046	Bal.	25.4	19.2	0.11	-	0.84	0.55	-	0.05	0.040	-
Alloy 625	0.015	4.3	22.5	Bal.	9.1	3.5	0.07	0.20	0.2	0.07	0.030	0.3
Kanthal APMT	0.080	Bal.	21.0	-	3.0	-	0.40	0.70	5.0	-	-	-

5.2 Field exposures

In a field exposure, samples are exposed to the real environment in a boiler. All field tests included in this thesis were performed at the Idbäcken power plant in Nyköping. For all exposures, initial corrosion was studied since rather short exposure times were used in the tests).

5.2.1 Furnace wall exposures at the Idbäcken power plant

The Idbäcken power plant is a BFB-boiler with a 63 MW thermal capacity for combined heat and power. For all tests in this thesis, the boiler was run on used-wood fuel and the tested materials were 16Mo3, 310S, nickel-base Alloy 625 and FeCrAl alloy Kanthal APMT, with chemical compositions as shown in Table 3. The test duration was 14.25 h, and the metal temperatures tested were 350 °C (16Mo3 and 310S, Paper II) and 400 °C (Alloy 625 and Kanthal APMT, Paper I).

Rectangular samples of the materials were exposed on an air-cooled probe as illustrated in Figure 7. The dimensions of the samples were 48 mm (length) x 7 mm (width) x 6 mm (thickness). Four samples were mounted on one probe, and a hole was drilled in the middle of each sample in order to measure the sample temperature with a thermocouple during exposure. The sample probe was rotated 90°, relative to the illustration in Figure 7, in a slit between two wall tubes during exposure. The samples were exposed at furnace wall position.

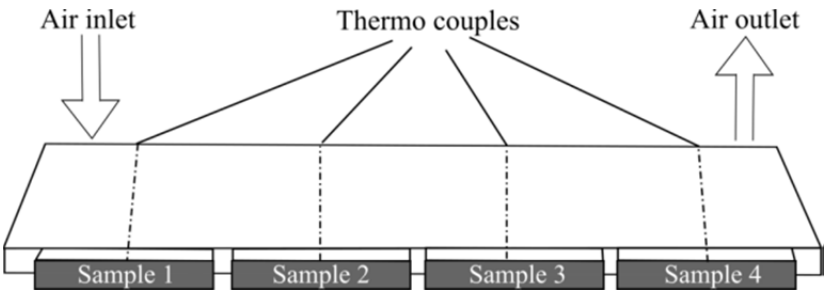

Figure 7. Illustration of furnace wall probe.

In one test-campaign, an additive of municipal sewage sludge was co-fired with the used-wood fuel to determine whether or not the additive decreased the corrosion of the tested materials. Samples were exposed identically to the test with 100 % used-wood fuel, except for the addition of municipal sewage sludge (8.4 wt%).

5.3 Laboratory exposure

In a laboratory exposure, it is possible to perform tests that are simplified compared to the otherwise very complex environment in a boiler. This is important in order to understand how a specific parameter influences the corrosion observed in the field. In this thesis, laboratory exposures were performed in order to study the influence of the lead content in a wood fuel on the initial corrosion of selected materials at the furnace wall position. The tests were performed in a laboratory fluidised bed boiler with synthetically made used-wood fuels.

5.3.1 Furnace wall exposures in laboratory fluidised bed boiler

The laboratory test rig used in these tests was a miniature boiler (10kW) in which a fuel is combusted in a fluidised bed. Pelletized fuel is fed to the bed from the side, and temperatures of the bed, flue gas and exposed metal samples are monitored during exposure. The test rig height was 3 m, and the reactor in which the samples were exposed had an inner diameter of 10 cm. The furnace wall position in this test rig was located between the secondary and tertiary air inlet. The composition of the flue gas was measured at the outlet of the boiler after the superheater position. A schematic illustration of the laboratory test rig is presented in Figure 8a.

In this thesis, the furnace wall position with a reducing condition (measured excess air ratio, λ=0.7) was studied. The flue gas temperature at the furnace wall position was in the range of 930 °C ± 8 °C during all test cases, and the metal temperatures tested were 350 °C and 400 °C. The exposed materials were the low-alloyed steel 16Mo3, the stainless steel 304L and the nickel-base Alloy 625, with chemical compositions as shown in Table 3. Ring-shaped samples with an outer diameter of 25 mm, an inner

diameter of 16 mm and a width of 10 mm were exposed in the tests. The samples were mounted adjacent to each other on an air-cooled probe, (see the illustration in Figure 8b), and, before being exposed to the flue gas, the probe was preheated to the desired test temperature. The metal temperatures were measured and regulated on a fourth ring sample located adjacent to the other samples at the innermost (towards the wall of the boiler) position on the probe.

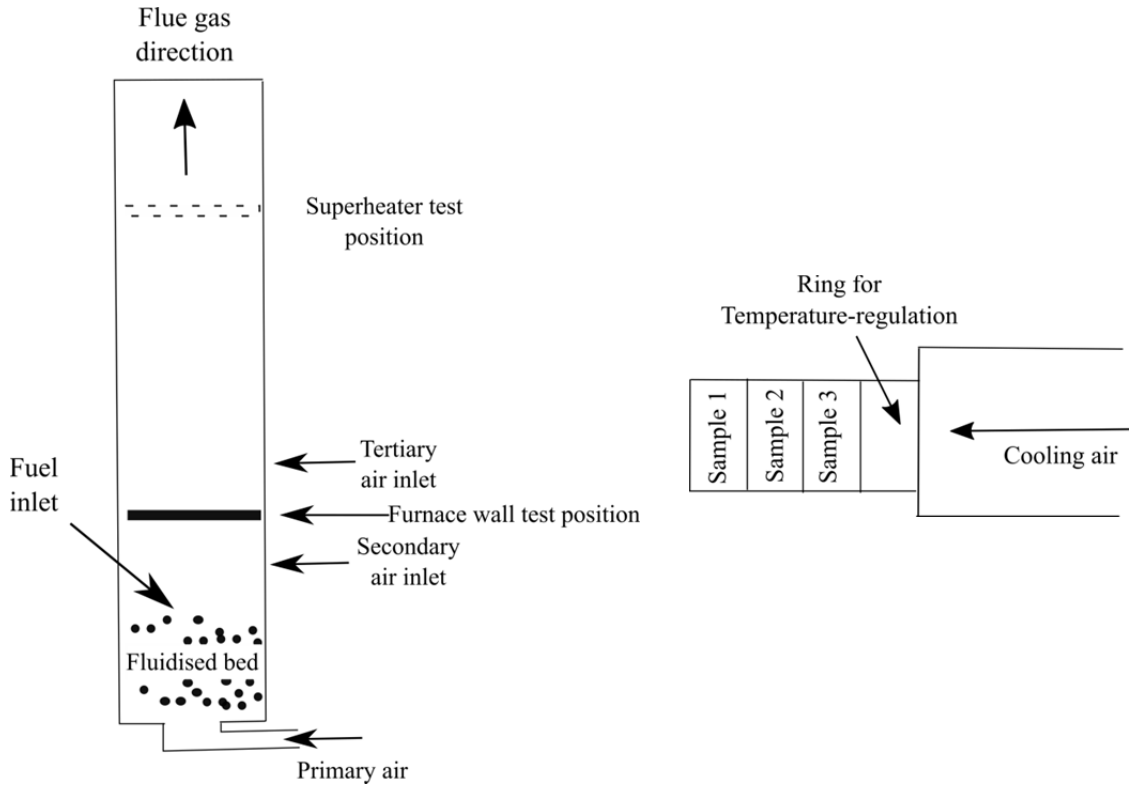

Figure 8. Illustration of a) the laboratory fluidised bed boiler and b) the probe with samples after exposure.

The fuels used in these tests were based on a reference wood fuel with low concentration of corrosive elements. In order to vary the amount of different key elements in the fuels, amounts of PbO, ZnO, KCl and polyvinyl chloride (PVC) were added. Three fuel mixtures with a variation in lead concentrations were prepared in order to simulate three different firing cases (L1-L3). In all these fuels, the added amounts of the key elements Cl, K, and Zn were kept constant. Two reference firing cases were conducted at 350 °C (R1 and R2). In reference case 1 (R1), the fuel used

was the reference wood pellet fuel (fuel R1) with no further additions of key elements. In reference case 2 (R2), the fuel composition was the same as in firing case L2 except for the exclusion of the ZnO additive. Table 4 shows the amounts of Pb, Zn, Cl and K added to the different fuels.

Table 4. Amounts of Pb, Cl, Zn and K added to the fuels.

		R1	R2	L1	L2	L3
Pb	mg/kg	0	100	10	100	1000
Cl	mg/kg	0	1000	1000	1000	1000
Zn	mg/kg	0	0	200	200	200
K	mg/kg	0	500	500	500	500

The flue gas was measured at the outlet of the furnace and, for all tests, the composition was 4 ppm SO_2, 5 vol% O_2, 10 vol% water and 45 ppm HCl except for the R1 case in which the HCl concentration was 3 ppm.

5.4 Fuel compositions

The focus of this study is on the initial corrosion of materials exposed to used-wood fuels. Several fuels were used throughout the field and laboratory tests performed in this thesis, (see Table 5).

Table 5. Numbering of fuels tested in the different exposures.

Fuel description	#	Exposure
100 % Used-wood fuel (typical, 30 days average)	A	Field
100 % Used-wood fuel (specific batch)	B	
Used-wood fuel+ 8.4 wt% sewage sludge addition (specific batch)	C	
100 % Used-wood fuel (specific batch)	D	
Wood pellets used in laboratory test (+additives L1, L2, L3)	R1 (L1, L2, L3)	Laboratory

The composition of the fuels varies slightly and the compositions for the different fuels are given in Table 6.

The main differences in fuel composition are seen for the C-fuel, to which sludge is added, and for the R1-fuel which is a wood pellet fuel. For the sludge fuel, the concentration of Si, Ca, Al, Mg and P are higher than what normally is measured for used-wood fuels. This is due to the presence of these elements in the sludge which, in this specific test, was tested with the aim to investigate how the presence of the sludge affects the corrosion behaviour of the materials. The general level of contaminants are low in pelletized wood fuel compared to used-wood fuel, and this was desirable since more controlled tests with the controlled addition of key elements were performed in the laboratory using this fuel. The varying component in this test was lead for which the concentrations tested were in the interval of 2 - 1002 mg/kg fuel.

Table 6. Composition of fuels exposed in the different tests described in Table 5.

	A	**B**	**C**	**D**	**REF 1**	**L1**	**L2**	**L3**
Moisture, 105 °C	22.9	30	38.8	30.7	9.7	9.7	9.7	9.7
Ash, 550 °C (% dry fuel)	3.2	5.1	11.7	5.8	0.5	0.5	0.5	0.5
C (%, dry fuel)	48.4	49	44.8	46.9	50.9	50.9	50.9	50.9
H (%, dry fuel)	5.9	6	5.5	5.7	6.3	6.3	6.3	6.3
N (%, dry fuel)	1.57	1.95	2.42	1.98	<0.10	<0.10	<0.10	<0.10
O (%, dry fuel)	40.8	40.2	35.3	39.4	42.2	42.2	42.2	42.2
S (%, dry fuel)	0.061	0.05	0.125	0.105	<0.012	<0.012	<0.012	<0.012
Cl (%, dry fuel)	0.08	0.1	0.16	0.06	<0.02	0.1	0.1	0.1
Si (mg/kg, dry fuel)	5250	2680	23700	12300	707	707	707	707
K (mg/kg, dry fuel)	1060	802	2330	945	367	867	867	867
Ca (mg/kg, dry fuel)	4020	3100	9510	6160	511	511	511	511
Al (mg/kg, dry fuel)	963	668	5760	2080	59.3	59.3	59.3	59.3
Na (mg/kg, dry fuel)	766	533	1610	1670	24.4	24.4	24.4	24.4
Mg (mg/kg, dry fuel)	437	356	1630	990	103	103	103	103
P (mg/kg, dry fuel)	116	78.4	1820	138	33.2	33.2	33.2	33.2
As (mg/kg, dry fuel)	17.2	14.2	21.5	14.3	<0.1	<0.1	<0.1	<0.1
B (mg/kg, dry fuel)	8.91	8.89	16.1	11.8	1.38	1.38	1.38	1.38
Cu (mg/kg, dry fuel)	29.4	34.3	53.3	26.7	31.9	31.9	31.9	31.9
Pb (mg/kg, dry fuel)	113	131	180	206	2.03	12	102	1002
Zn (mg/kg, dry fuel)	56.4	65.8	200	494	40.9	240.9	240.9	240.9

Of the three used-wood fuels, the largest deviation was observed for the D-fuel for which slightly higher amounts of Pb and Zn were measured than for the other 100 % used-wood fuel batches (A- and B-fuel). The corrosion behaviour of samples exposed to this fuel is included in order to verify some of the features observed in the laboratory exposures.

5.5 Post-exposure sample preparation and analyses

After exposure, the samples were investigated with the different techniques presented in Chapter 4. Different sample types were exposed in the field tests and the laboratory tests, and, thus, the samples were prepared in different ways after exposure.

5.5.1 Surface analysis

The surface of the deposits was studied with the use of SEM/EDS and XRD. For all samples, the SEM/EDS analyses were performed on the surface before any cutting took place. The analyses were performed at windward position and 2-4 areas each of 5 mm^2 were analysed on every specimen, (see Figure 9). All SEM images presented in the thesis were obtained with backscatter detector.

XRD evaluation was performed on scraped-off deposits of the ring samples exposed in the laboratory tests and the probe samples of Alloy 625 and FeCrAl alloy Kanthal APMT exposed in the field tests. For the other probe samples (16Mo3 and 310S) exposed in the field tests, XRD analysis was performed directly on the outermost surface of the samples.

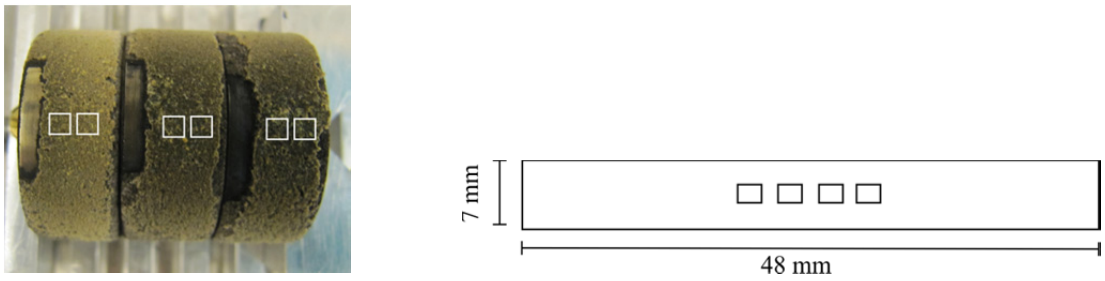

a) b)

Figure 9. Illustration of areas for surface analysis on a) ring samples and b) probe samples.

5.5.2 Cross sectioning analyses

Slightly different techniques were used in the sample preparation of the samples due to differences in shape. The general procedure was the following; dry cutting perpendicular to the surface, hot embedment and dry grinding. For a few samples (Alloy 625 and Kanthal AMPT in the field exposure), a 45 °grind was prepared as well without any embedding of the sample. The findings from these are included in Paper I. Figure 10 and Figure 11 show illustrations of the cross sectioning and grinding of the samples.

The cross sections were evaluated with the use of imaging in SEM and chemical analyses performed with the use of EDS. Both local analyses and mapping analyses were performed, and the acceleration voltage used was mainly 20 keV. As a complement to the EDS analysis, the WDS technique was used in order to separate Mo, S and Pb, which can be difficult to do with the EDS technique due to overlapping signals.

Figure 10. Cross sectioning of a) ring sample and b) rectangular sample.

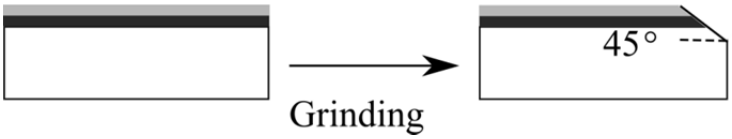

Figure 11. Illustration of 45° cross grinding of rectangular probe sample.

5.5.3 Chemical depth analysis

The probe samples were also evaluated with the use of glow discharged optical emission spectroscopy (GD-OES). In this equipment, the samples must have a certain size in order to fit the O-rings in the system (to maintain vacuum in the system during the analysis). Thus, when such a small sample size is used, the sample must be embedded in a Sn/Bi mould in order to form a larger sample that fits in the system, (see Figure 12).

a) *b)*

Figure 12. Sample preparation procedure for GD-OES samples a) after embedment in Sn/Bi and b) sample after sputtering and removal from the embedded material.

6 Results and discussion

6.1 Influence of lead content in wood fuels

As described in the introduction, the lead content in used-wood fuels is believed to affect the corrosion of metallic materials. In a laboratory fluidised bed boiler, three materials, 16Mo3, 304L and Alloy 625, were exposed to three fuel mixtures with a variation in lead content (Paper III). Exposures were performed at 350 °C and 400 °C for 8 hours.

6.1.1 Deposit appearance and general observations

The general deposit appearance in a cross section of all the samples was a layered structure after exposure at 350 °C, (see Figure 13). In all cases, independent of lead concentration, an outer layer of potassium chloride was found, and underneath, the layers were enriched in lead.

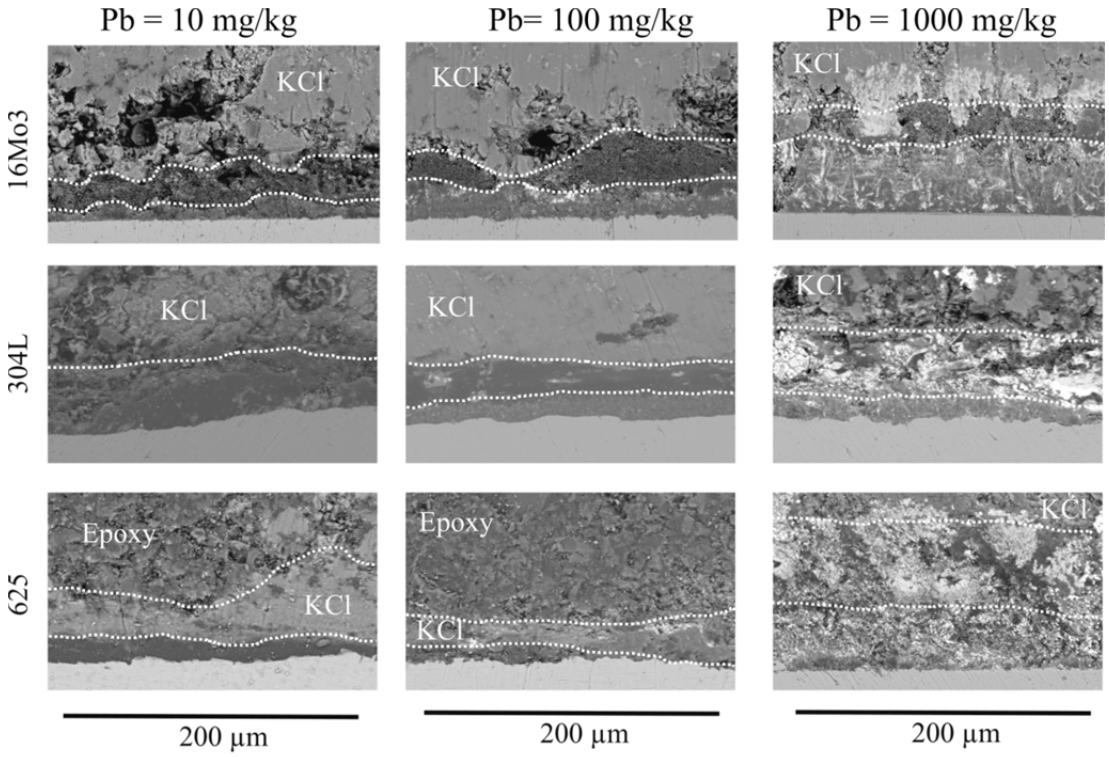

Figure 13. Deposit structure of samples exposed at 350 °C to a wood fuel with variations in lead content at furnace position. Layers are separated with dotted lines.

The lead compounds appeared to be drawn towards the metal surface (bright areas in the figures). Chemical analysis of key elements (Cl, K, Na, Zn and Pb) in the deposit layers confirmed this increase since the measured lead concentration was the highest in the layer closest to the metal substrate, (see example for 16Mo3 in Figure 14).

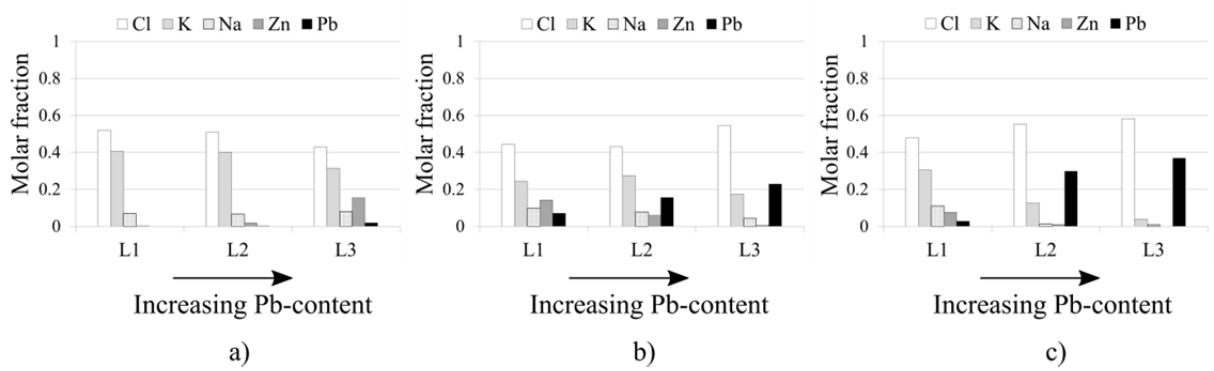

Figure 14. Molar fraction of corrosive elements in deposit layers on 16Mo3 a) outermost layer, b) middle layer and c) innermost deposit layer.

Surface analysis of the deposit using SEM/EDS showed similar results where, except for oxygen, chlorine and potassium comprised most of the deposit, (see example for 304L in Figure 15a). With increasing lead concentration in the fuel, lead increased in the surface deposit on all materials for both metal temperatures, (see Figure 15b).

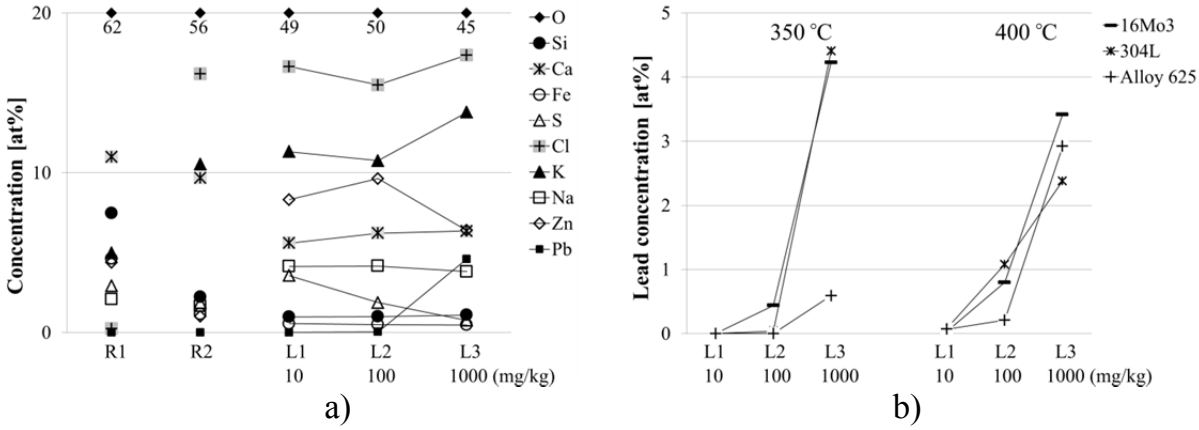

Figure 15. Surface analysis of a) deposits on 304L samples at 350 °C and b) all samples with respect to lead content in the deposit.

The samples exposed to reference fuel R1 (only wood pellets) at 350 °C showed low concentrations of corrosive elements in the surface deposit, while the sample for which

all additives except ZnO were included in the fuel (R2), showed an increase in K and Cl in the surface deposit. Furthermore, the samples exposed to reference fuel R1 showed negliable corrosion and the samples exposed to reference fuel R2 behaved in a similar manner as the samples exposed to the L2 fuel.

The findings from the SEM/EDS analyses were strengthened with the XRD analysis of scraped-off deposits, which at both metal temperatures and for all materials showed that the main compound present in the deposits is potassium chloride, (see Table 7). The lead compounds that occurred in the deposit at the highest lead concentration were identified to mainly be lead, lead/potassium-chloride, lead oxychlorides and lead oxide. It is not likely that these compounds co-exist in equilibrium in the deposit due to differences in stability with respect to partial pressures of oxygen and chlorine. However, since the deposits were scraped off the sample and mortared prior to analysis, they appear together in the findings.

Table 7. Detected crystalline phases in the deposits, representative for all materials.

		R1[1]	**R2**[1]	**L1**	**L2**	**L3**
350 °C	strong	SiO_2	KCl	KCl	KCl	KCl
	medium	KCl, NaCl, $K_3Na(SO_4)_2$	NaCl	NaCl, ZnO	NaCl, ZnO	Pb, ZnO, KPb_2Cl_5, NaCl
	weak	$K_2Ca_2(SO_4)_3$	$Ca(SO_4)$, Pb	$Ca(SO_4)$, Pb	$Ca(SO_4)$, Pb	PbO, Pb_2O_2Cl
400 °C	strong			KCl	KCl	KCl
	medium	Not exposed	Not exposed	NaCl, ZnO	NaCl, ZnO	Pb, ZnO, NaCl, PbO, Pb_2O_2Cl, $Pb_3O_2Cl_2$[2]
	weak			$Ca(SO_4)$, Pb	Pb, $Ca(SO_4)$	-

[1] Only analysed for 16Mo3

[2] Only observed for Alloy 625

A simplified thermodynamic diagram was constructed with the use of Thermo Calc® software and the SSUB3 database to study the stabilities of the different Pb-O-Cl containing compounds. The diagram shows the stability of the different compounds, with respect to oxygen and chlorine partial pressure, (see Figure 16). One of the lead oxychlorides identified with XRD, Pb_2O_2Cl, could not be found in the databases available, but other studies have proven its existence with XRD analysis [48]. It is, consequently, not unlikely that this compound could form.

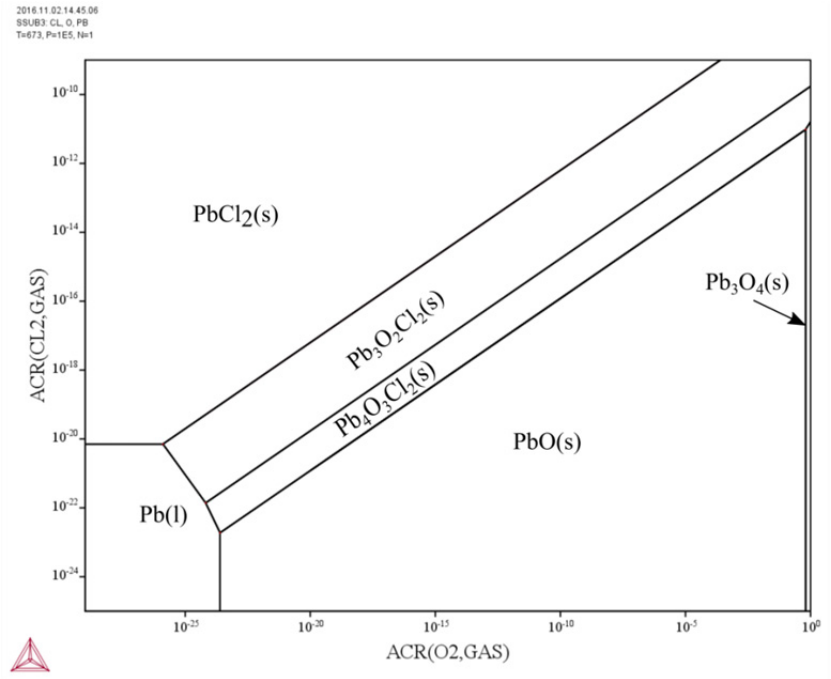

Figure 16. Stable phases of compounds including Pb, Cl and O as a function of chlorine and oxygen partial pressure at 400 °C.

Zink oxide was present in the deposits for all firing cases except for R1. In the cross sections at 350 °C, ZnO was found within the potassium chloride layer, (see Figure 17). No zinc chloride is found in the deposit at any of the tested metal temperatures, thus, the main zinc compound in the deposit seems to be zinc oxide. This compound has been shown to be less corrosive at 550 °C than zinc chloride at 350 °C and 450 °C, [36], and is not believed to influence the findings in this study significantly.

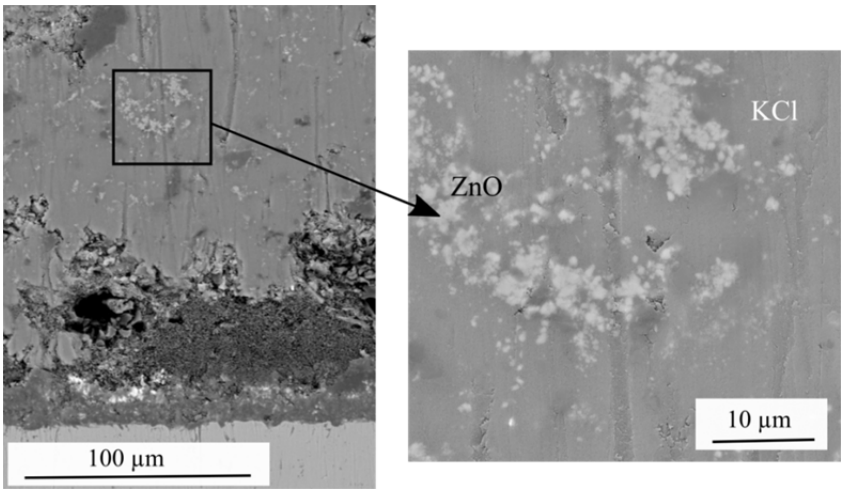

Figure 17.Cross section of 16Mo3 exposed to fuel with a lead concentration of 100 mg/kg illustrating the location of ZnO areas in the deposit.

6.1.2 Low-alloyed steels

Already at 350 °C, the low-alloyed steel corroded even though the corrosion was minor. A thin iron oxide was present on the samples after exposure to all the tested lead concentrations in the fuel and is assumed to be a result of corrosion, (see Figure 18). At the highest lead concentration, 1000 mg/kg fuel, this oxide was slightly thicker (up to 3 µm) than when the lead concentration was 10 mg/kg and 100 mg/kg, which indicates an increase in corrosion with lead content in the fuel. Also, the oxide was continuous at the highest lead concentration while it more sporadically occurred in the other cases. In addition, lead-rich areas were present close to the oxide, and these areas increased in number when the lead content in the fuel increased.

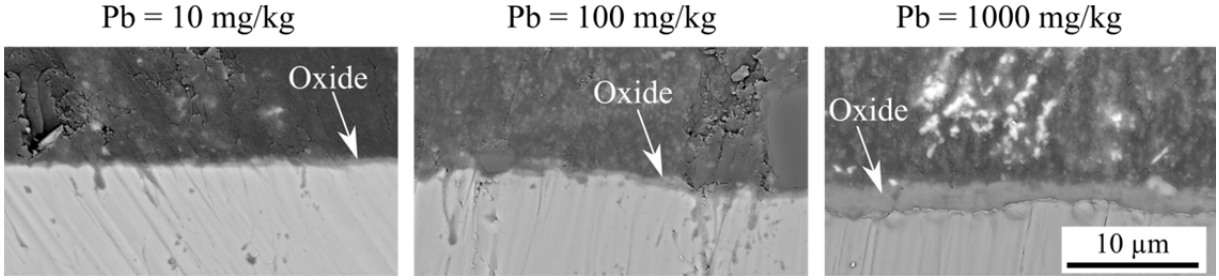

Figure 18. Cross section of 16Mo3 showing oxide formation when exposed to a wood fuel with different lead concentrations at 350 °C for 8 h.

At 400 °C, the increased lead content in the wood fuel had a clear effect on the corrosion behaviour of the low-alloyed steel, and the corrosion products formed for all the firing cases were iron chloride and iron oxide. The appearance of the corrosion products is illustrated in Figure 19. When the lead concentration was 10 mg/kg in the fuel, iron chloride was located closest to the metal substrate with a continuous layer of iron oxide on top. Thick oxide islands were found sporadically on the continuous iron oxide layer, resulting in an average oxide thickness of 25 µm. Increasing the lead content to 100 mg/kg in the fuel resulted in an average oxide thickness of approximately 120 µm. The oxide layer closest to the iron chloride was thicker, and an increased number of oxide islands were observed. An even higher lead concentration in the fuel (1000 mg/kg), however, did not give any additional increase in average oxide thickness; instead the oxide islands grew in a lateral direction forming a layer like structure. This increased oxide formation in the lateral direction is related to a weight increase (see Paper III), which indicates an increase in corrosion even though a thicker oxide was not measured.

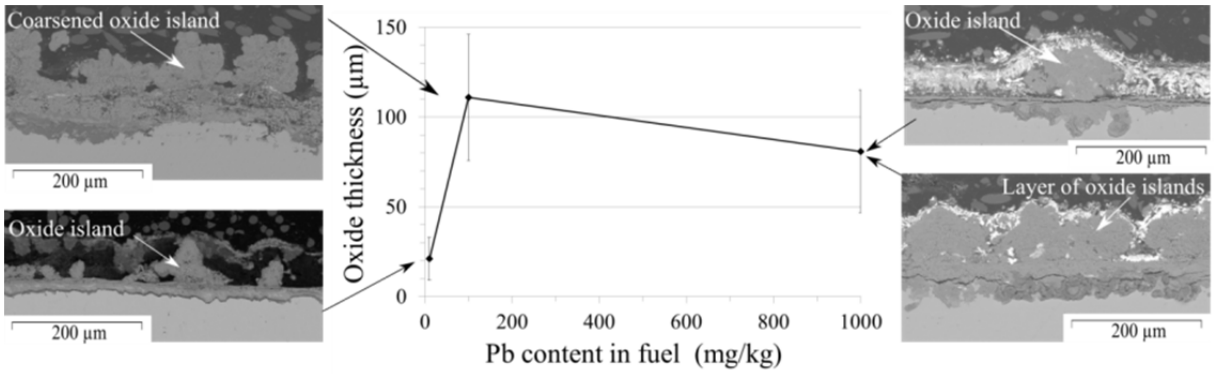

Figure 19.Oxide appearance and thickness vs. Pb content in the fuel for 16Mo3. The error bars represent the standard deviation of the oxide thickness for each sample.

A clear temperature dependence was observed for the low-alloyed steel since the corrosion increased from minor (oxide thicknesses of a few µm) at 350 °C to severe (oxide thicknesses of 25–120 µm) at 400 °C. However, it was not only the temperature that accelerated the corrosion; an increase in lead content in the fuel resulted in an

accelerated effect. This gives reason to believe that an additional corrosion mechanism related to lead compounds in the deposit has been active at 400 °C.

The lead compound added to the fuel was lead oxide, and considering the reducing conditions at the furnace wall position, lead oxide should be reduced to lead. According to thermodynamic calculations by Enestam et al. [23] both lead and lead oxide are possible to condense on tube surfaces within the metal temperature range tested in this study. Whether or not lead or lead oxide condenses, however, depends on the conditions. At oxidising conditions, lead oxide is likely to condense, and during reducing conditions, metallic lead is more likely to condense. Considering the reducing conditions that prevailed in this study and the metal temperatures, metallic lead should condense as liquid lead on the tube surfaces due to the low melting point of lead (327 °C [32]). On the other hand, the condition at the sample position probably fluctuated between reducing and oxidising throughout the test period, and it is not unlikely that also lead oxide condensed on the sample surfaces. Besides condensation, deposition of particles is possible as well.

According to the XRD results, both lead and lead oxide were present in the deposits. Considering that the corrosion products observed for 16Mo3 already at the lowest lead concentration were iron chloride closest to the metal substrate and iron oxide on top, it is likely that the main cause of the corrosion was chlorine-induced at this low lead concentration. This corrosion behaviour has been reported by other authors as well for this material [47], and the corrosion mechanism that causes this corrosion has been widely studied and is discussed in Subchapter 3.2.1.

An additional corrosion process that involves a reaction of lead oxide and/or metallic lead with the initially formed iron chloride is proposed to explain the further oxide growth when the lead content in the fuel (Paper III) increases. The driving forces for such reactions are strong and result in the formation of iron oxides (both Fe_2O_3 and Fe_3O_4 are possible) and lead chloride, (see Equation (12) and (13)) [32].

$$PbO(s) + FeCl_2(g) + 1/6\ O_2(g) = 1/3\ Fe_3O_4(s) + PbCl_2(s) \quad \Delta G^0_f = -149\ kJ/mol \qquad (12)$$

$$Pb(l) + FeCl_2(g) + 2/3\ O_2(g) = 1/3\ Fe_3O_4(s) + PbCl_2(s) \quad \Delta G^0_f = -301\ kJ/mol \qquad (13)$$

Assuming that the initially formed iron chloride evaporates through the oxide layer, as suggested by the mechanisms for active oxidation, and meets the lead oxide, this process results in the formation of lead- and chloride-containing compounds further out in the deposit. Also, in combination with potassium chloride, the lead chloride could form a low melting salt mixture of KCl and $PbCl_2$ (T_m=411 °C, Figure 21 [33]), which would increase the risk of corrosion even further.

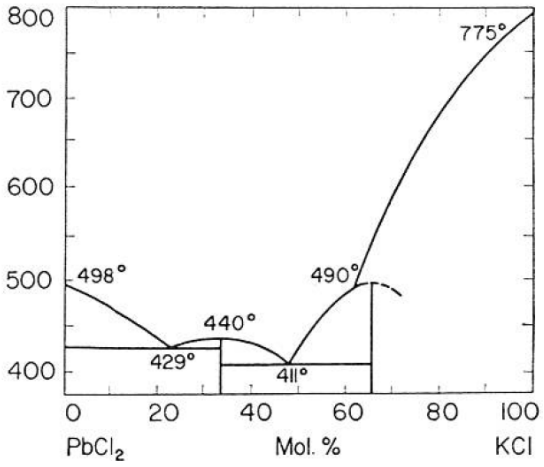

Figure 20. Binary phase diagram of $PbCl_2$ and KCl [33].

This is actually what was seen in cross sections of the corroded 16Mo3-samples, (see Figure 21). On top of the oxide layer, lead and chlorine are present in combination with oxygen. In the middle of the oxide (where the temperature is higher than at the metal substrate), areas with a multiphase structure is present. This structure has a composition indicating an eutectic mixture of KCl and $PbCl_2$ since the molar ratio of Pb to K is 1:1 according to SEM/EDS analysis. In the binary phase diagram of these salts, the composition of the lowest melting salt mixture has similar molar ratios, (see Figure 20).

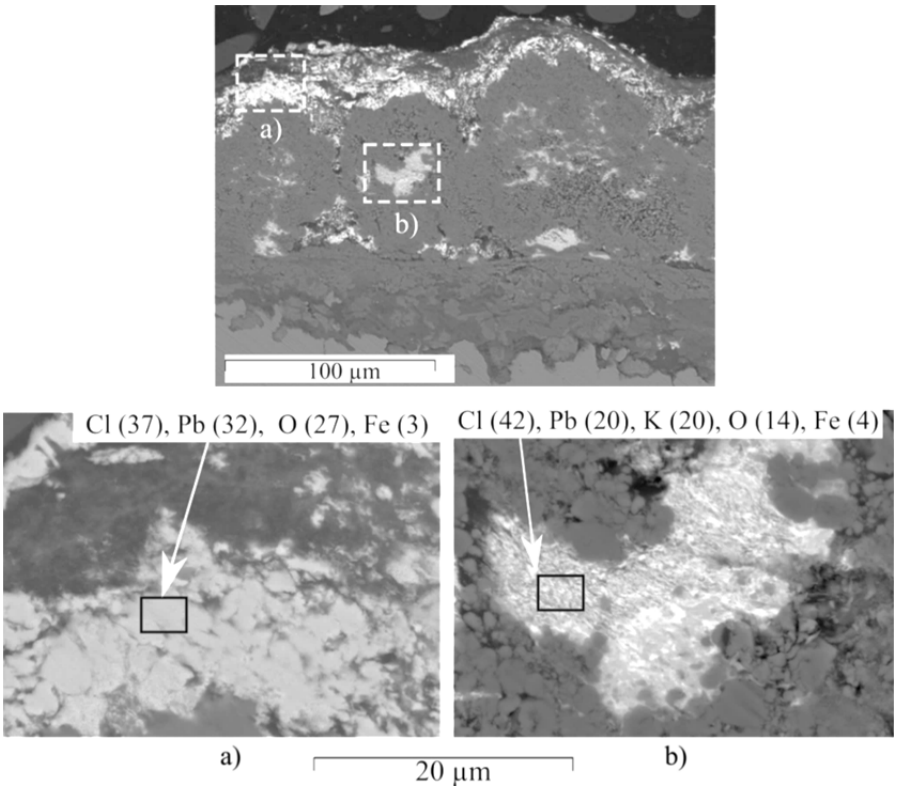

Figure 21. Cross section of 16Mo3 exposed to a wood fuel with 1000 mg/kg Pb a) Cl-Pb-O compounds on top of oxide and b) Cl-Pb-K compound within the oxide,(at%)

The behaviour with low melting salt areas present in the interior of the oxide can be seen for both the firing case with 100 mg/kg and the case with 1000 mg/kg Pb in the fuel, but the amount of these possibly molten areas clearly increases in amount when the metal is exposed to the highest concentration. The presence of these areas indicates that the salt mixture was molten during exposure, which can explain the high corrosion rates observed. This multiphase, possibly eutectic, structure should, according to the phase diagram of $PbCl_2$ and KCl, consist of PbK_2Cl_4 and KPb_2Cl_5 [49]. According to thermodynamic calculations, at fairly similar conditions, these compounds were predicted to be formed in the deposit [22]. These At 400 °C, none of these compounds were, however, confirmed with XRD. The main part of the two-phase structure was located in the interior of an oxide, which did not show strong signals in the XRD spectra. Most probably this means that most of the oxide and, consequently, also the two-phase structure remained on the samples when the deposit was scraped off. At 350 °C, KPb_2Cl_5 was confirmed with XRD in deposits from samples exposed to the fuel

with the highest lead concentration (1000 mg/kg fuel). No signs of the melt were, however, found at this temperature, but this was not expected anyway since the metal temperature was clearly lower than the melting point of this salt mixture (411 °C [33]).

The lead chloride proposed to form in Equation (12) and (13) was not detected with X-ray diffraction (XRD), instead different lead oxychlorides were found in the deposit, (see Table 7). Also in the cross section and SEM/EDS analysis, an oxygen signal was present in the lead/chlorine-rich areas. It is, thus, reasonable to assume that the lead chloride formed reacted with oxygen and formed different types of lead oxychlorides.

6.1.3 Stainless steels

When the stainless steel 304L was exposed to the fuels with a variation in lead content in the laboratory test rig, no significant corrosion was observed at any of the metal temperatures tested. No measurable oxide was observed, only deposit was present on the samples. From the surface analysis performed with XRD and EDS, it could, though, be seen that lead compounds increased in number in the deposits when the lead concentration in the fuel increased. At the highest concentration and at a metal temperature of 400 °C, lead had migrated towards the metal substrate, (see cross section in Figure 22). Above the lead rich areas, potassium chloride was observed. This is similar to what was observed of the layered deposit structure at 350 °C.

Why clear corrosion was not observed for this material in this study could be due to the short exposure time. This material was expected to form a protective chromium oxide that is more protective than the iron oxide formed on the low-alloyed steel 16Mo3. Since no corrosion was observed for this material, a possible explanation is the formation of a chromium oxide even though this oxide would have to be very thin since it is not readily observable.

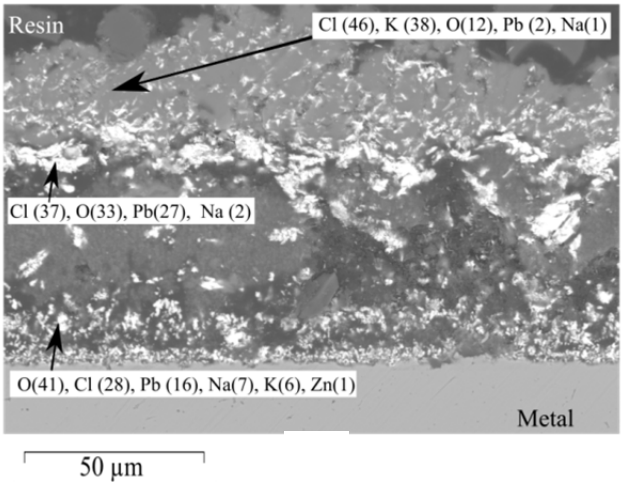

Figure 22. Cross section of 304L exposed to a fuel with a Pb concentration of 1000 mg/kg at 400 °C, chemical analysis in at%.

Comparing the results from this laboratory exposure with results from the field test where the higher alloyed stainless steel, 310S, was exposed to a used-wood fuel with a lead concentration of 200 mg/kg (fuel D in Table 6) for 14 h at two temperatures, similar results regarding the lead distribution in the deposit were observed. The samples were investigated using the FIB technique. At 350 °C, (see Figure 23), no clear oxide formation, which would indicate corrosion, was observed, however, lead-rich areas (the bright areas in the figure) were observed close to the metal substrate.

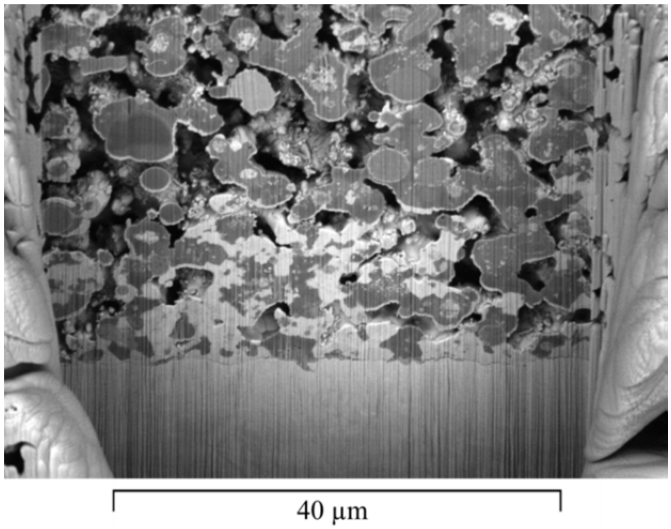

Figure 23. FIB-milled cross section of 310S exposed to used-wood fuel, metal temperature 350 °C.

At 400 °C, areas with a Pb-rich deposit were observed close to the metal substrate as well, (see Figure 24). At this temperature, corrosion occurred with oxide formation as a result. Comparing images of two areas of a FIB cross section it was found that the oxide appeared to be thicker in connection to areas with a lead-rich deposit compared to areas not as rich in lead, (see Figure 24). These findings strongly indicate that an increase in lead compounds close to the metal substrate pose a risk for corrosion with time for the stainless steels.

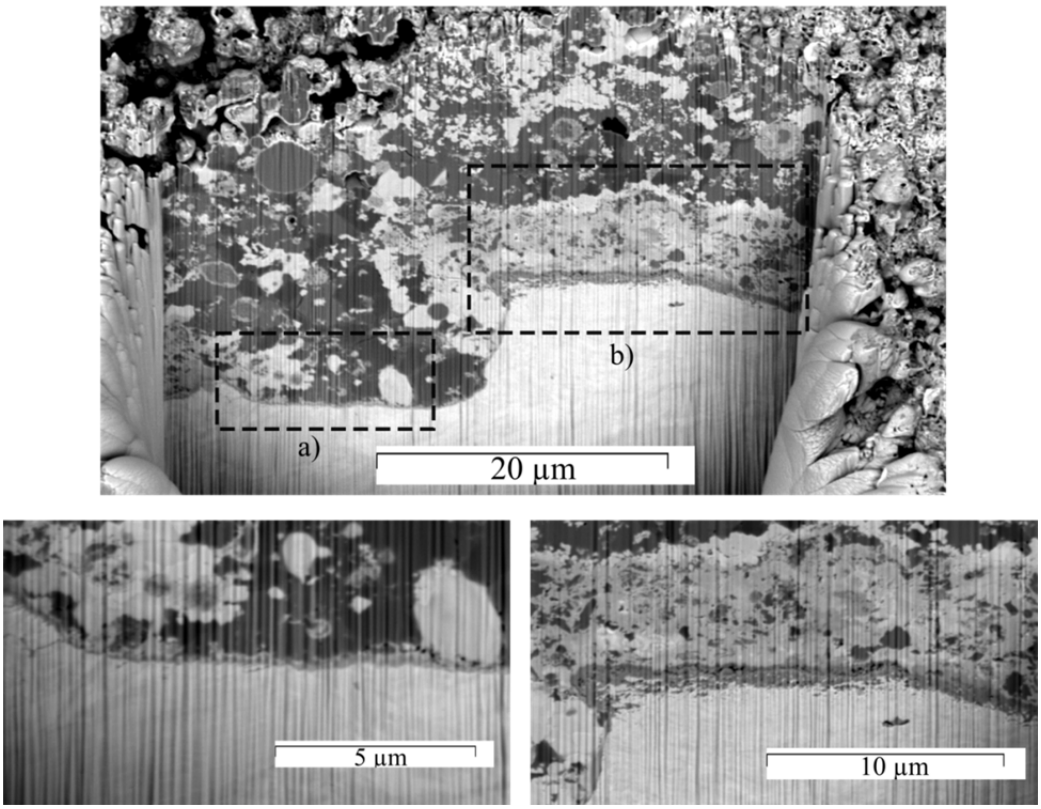

Figure 24. FIB-milled cross section of 310S exposed to used-wood fuel, metal temperature 400 °C.

6.1.4 Nickel-base alloys

At both 350 °C and 400 °C, a migration of lead rich compounds towards the metal substrate was observed for the nickel-base alloy 625. The migration of lead was more pronounced at 400 °C, as can be seen in Figure 25 (compared to Figure 13). Despite

this Pb-migration towards the metal surface, no measurable corrosion was observed for this material at any of the tested metal temperatures. However, due to the corrosive deposit close to the metal substrate, corrosion cannot be excluded from a longer time perspective.

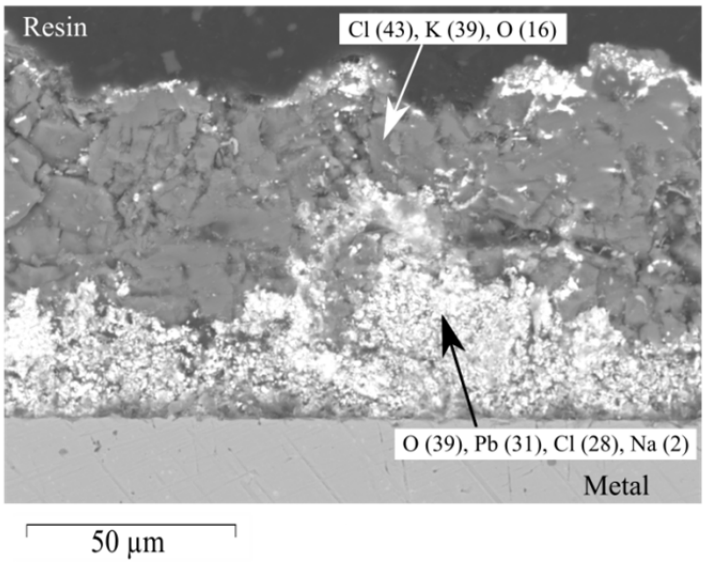

Figure 25. Cross section of Alloy 625 exposed to fuel with Pb concentration of 1000 mg/kg at 400 °C.

The lead-rich compounds in the deposit for Alloy 625 and 304L were found to contain a high amount of chlorine and oxygen. According to the XRD analysis, lead oxychlorides are present in the deposits of all these materials, which is most probably what was observed in the cross sections in the EDS analysis. For 16Mo3, it is proposed that the reaction of lead oxide or pure lead with iron chloride is important for the corrosion mechanism to form iron oxide and lead chloride. Lead chloride is then believed to further react with oxygen and form the lead oxychlorides.

The presence of lead oxychlorides in the deposit for Alloy 625 (and 304L), in which no measurable corrosion was observed, indicates that lead chloride can be formed in another way as well. The condensation of lead chloride is expected at metal surfaces in the temperature range of 186-334 °C when the metal is exposed to reducing conditions similar to the ones in this study [23]. For this reason, lead chloride is not expected to be present in the deposits in this laboratory study as a result of condensation from the

flue gas. However, the condensation temperature increases with an increase in the partial pressure of lead in the flue gas, and in oxidising conditions, this condensation is expected in the temperature interval of 338-420 °C [23]. Consequently, the condensation of $PbCl_2$ cannot be excluded since the conditions are believed to fluctuate at furnace wall position, resulting in alternating reducing and oxidising conditions. Also, the migration of lead towards the metal substrate does not seem to be a result of corrosion since negligible corrosion was measured for the high-alloyed materials. This migration is instead believed to be an effect of a thermal gradient and/or variations in chlorine and oxygen partial pressure throughout the deposit.

6.2 Influence of sewage sludge additive

One way to decrease furnace wall corrosion when firing with used-wood fuel is to change the environment in the boiler by co-firing an additive with the fuel. In a field test campaign, the effect of municipal sewage sludge was evaluated by comparing the corrosion of samples exposed to 100% used-wood fuel with samples exposed to a combination of used-wood fuel and sewage sludge additive. Four materials were exposed at furnace wall position for 14 h at metal temperatures of 350 °C (16Mo3 and 310S, Paper II) and 400 °C (Alloy 625 and alumina-forming Kanthal APMT, Paper I).

6.2.1 Deposit appearance and general observations

When sewage sludge was co-fired with used-wood fuels, corrosive species like alkali, chlorine and heavy metals decreased in the deposits, (see
Table 8). At the same time, the elements aluminium and silica increased. This indicates that the addition of sludge has a positive effect on decreasing the corrosive species in a deposit and, consequently, decreasing the risk for corrosion.

Table 8. Average chemical composition (wt%) of surface deposits.

Fuel*	O	Na	Mg	Al	Si	P	S	Cl	K	Ca	Ti	Mn	Fe	Cu	Zn	Pb
16Mo3																
UW	28.6	7.7	0.9	1.1	2.0	0.4	4.3	12.2	3.8	8.6	2.5	0.7	15.1	0.8	3.3	8.0
UW+S	46.1	3.2	1.8	2.4	4.7	1.7	5.3	3.7	3.3	14.1	3.9	0.3	4.3	0.0	3.2	1.9
310S																
UW	35.6	2.8	1.2	1.6	2.9	0.6	7.9	4.6	5.1	14.5	4.3	0.5	3.7	0.6	5.4	8.6
UW+S	43.7	4.2	1.4	3.5	3.6	1.8	6.6	2.7	4.4	11.2	3.0	0.2	4.9	0.3	3.7	4.7
Alloy 625																
UW	40.8	4.6	1.6	1.0	1.9	0.7	10.6	4.0	8.5	10.7	3.2	0.2	1.1	0.2	4.2	6.6
UW+S	42.1	4.0	1.4	4.5	3.5	1.8	6.6	3.1	5.0	10.8	2.9	0.2	4.3	0.3	3.3	6.0
Kantahl APMT																
UW	40.4	6.5	1.4	1.5	1.6	0.5	11.3	5.0	7.5	8.9	2.6	0.2	1.6	0.4	2.5	8.0
UW+S	44.7	3.7	1.6	2.7	3.5	1.8	7.1	2.3	5.0	12.3	3.2	0.2	4.4	0.0	3.6	3.3

* UW = used-wood fuel, UW+S = used wood fuel + sewage sludge

With the addition of sewage sludge, different sulphates increased in the deposits, (see XRD results in Table 9), and these have been shown to be less corrosive than, for instance, alkali chlorides [30]. It is suggested that alumina silicates capture alkali metals according to Equation (14). The compound $K_2Al_2S_{i2}O_8$ is found in the deposit of Kanthal AMPT when sewage sludge is co-fired with used-wood fuel and further indicates that the addition of sewage sludge to used-wood fuel has the desired effect.

$$Al_2O_3 \cdot 2SiO_2 + 2KCl + H_2O \rightarrow K_2O \cdot Al_2O_3 \cdot SiO_2 + 2HCl \qquad (14)$$

Table 9. Crystalline compounds present in the deposit detected with XRD.

	Fuel	Strong	Medium	Possible/indicated
16Mo3	UW	Fe_2O_3, Fe_3O_4, NaCl,	KCl, $CaSO_4$	$K_2Ca_2(SO_4)_3$
	UW+S	$CaSO_4$	Fe_2O_3, Fe_3O_4, KCl, NaCl, $K_2Ca_2(SO_4)_3$	-
310S	UW	Fe_3O_4, NaCl	KCl, Fe_2O_3, $Ca(SO_4)$, $K_2Ca_2(SO_4)_3$	Cr_2O_3
	UW+S	$CaSO_4$	Fe_2O_3, Fe_3O_4, NaCl, KCl, $K_2Ca_2(SO_4)_3$	Cr_2O_3
Alloy 625*	UW	NiO	$(Na,K)_2SO_4$	K_2SO_4, $K_2Pb(CrO_4)_2$
	UW+S	$K_2Ca_2(SO_4)_3$, Cr_2O_3	Unidentified	Fe_2O_3
Kantahl APMT*	UW	KCl, $CaCl_2$	$K_2Al_2O_4$	K_2PbO_2
	UW+S	KCl	$K_2Al_2Si_2O_8$	$K_2Ca_2(SO_4)_3$

* Scraped-off deposit

6.2.2 Low-alloyed steels

For the low-alloyed steel 16Mo3, the addition of sewage sludge to a used-wood fuel slightly decreased corrosion. In general, the layer of corrosion products was thicker on the sample exposed to 100% used-wood fuel than on the sample that was exposed to used-wood fuel with a sewage sludge addition. After cross sectioning, most of the deposit was spalled for the 100 % used-wood fuel sample, (see Figure 26), while for the sample exposed to the used-wood fuel with sewage sludge addition, the deposit was still present, (see Figure 27). Both with and without sewage sludge addition to used-wood fuel, the corrosion products on the samples consisted of iron chloride and

iron oxide as illustrated with chemical composition maps in Figure 28. The maps further confirm that very little deposit is present on the sample exposed to the 100% used-wood fuel. When sewage sludge is co-fired with used-wood fuel, less chlorine is found at the metal interface, which indicates less initial corrosion. In addition, it can be seen in Figure 28 that the thickness of the oxide is thinner on the sample exposed to the used-wood fuel with sewage sludge addition than on the sample when only used-wood is fired.

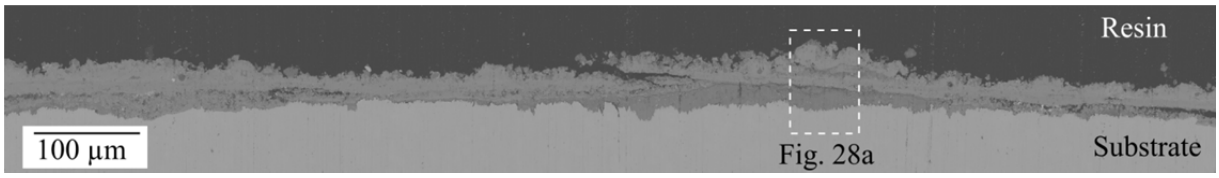

Figure 26. Cross section of 16Mo3 exposed to 100% used-wood fuel at 350 °C.

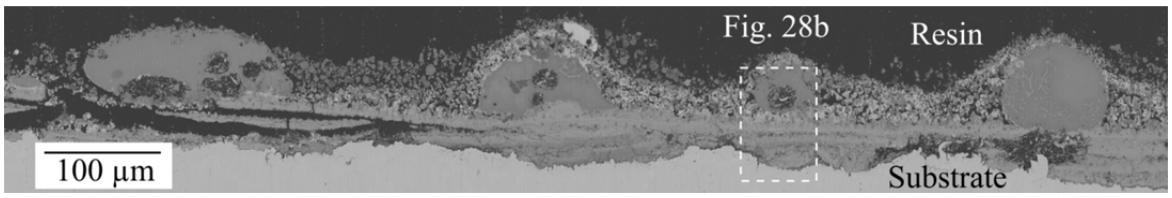

Figure 27. Cross section of 16Mo3 exposed to used-wood fuel and sewage sludge addition at 350 °C.

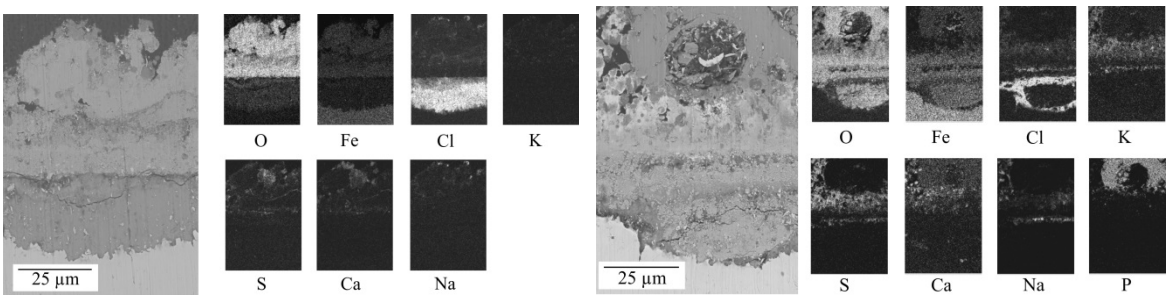

a) b)

Figure 28. Cross section of 16Mo3 samples exposed to a) 100 % used-wood fuel and b) used-wood fuel + sewage sludge. Both with elemental composition distribution

The presence of iron chloride as a corrosion product was confirmed for the specimen exposed to 100% used-wood fuel with the use of the FIB technique with combined energy dispersive spectrometry (EDS). With this technique, the specimen is cut in

vacuum, and directly after cutting, it is chemically analysed. In this way, the iron chloride is exposed to a minimal amount of oxygen or humidity, which otherwise can cause oxidation/hydration of the iron chloride, (see Figure 29).

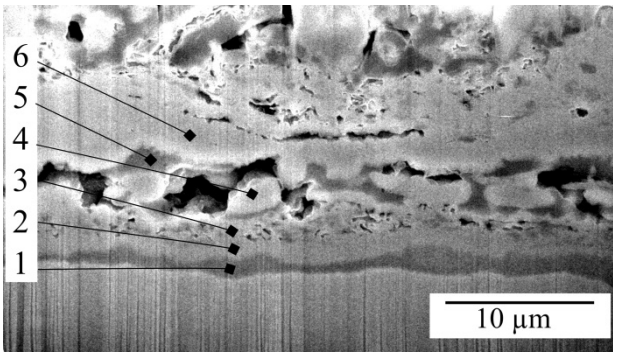

	O	S	Cl	K	Fe	Pb
1		0.4	33.2		65.2	0.1
2	24.4	1.4	8.3		65.7	0.2
3	29.4	0.8	2.1	1.1	66.0	0.2
4	26.9	0.4	1.9	0.8	69.8	0.2
5	7.0	0.6	23.3	20.1	42.7	0.3
6	27.5	0.3	0.9	0.6	70.5	0.2

Figure 29. FIB cross section of 16Mo3 exposed to 100% used-wood fuel at 350 °C with chemical composition given in at%.

Closest to the metal substrate in this figure, no oxygen can be seen in the corrosion product, which mainly consists of iron and chlorine. This cross section in FIB was performed at a spot where the deposit and corrosion product layers were thin due to the technique, which is preferably used for smaller/thinner cross sections because, otherwise, the procedure would be very time consuming.

Higher lead concentrations were measured in the surface deposit on the 100 % used-wood fuel samples. This was also observed in cross sections of the 16Mo3 specimen (Paper II) and was indicated with GD-OES analysis, (see Figure 30). An increase in lead signal was observed in the iron oxide layer for the sample exposed to 100 % used-wood fuel while no lead enrichment was observed for the sample exposed to the used-wood fuel with a sewage sludge addition. Since no signals from deposit elements S and Ca were found in the GD-OES spectra, this indicates that the deposit had spalled during the analysis. Results from the lead influence study (Subchapter 6.1) showed that lead compounds are often concentrated to the inner part of a deposit/oxide layer, and this is also indicated in the GD-OES spectra. A possible increase in lead content further out in the deposit of the sludge sample cannot be excluded based on the GD-OES-analysis, but an EDS analysis of the surface deposit indicated no such strong increase further out, (see

Table 8).

This decrease in lead content in the deposit on the sample with a sewage sludge additive indicates that the addition of sludge resulted in a decrease in the amount of lead compounds in the deposit. Since the lead content in the used-wood fuel combined with sewage sludge is higher than the 100 % used-wood fuel, (see Table 6), the idea that the effect of adding sewage sludge leads to a decrease in lead content in the deposit is further strengthened.

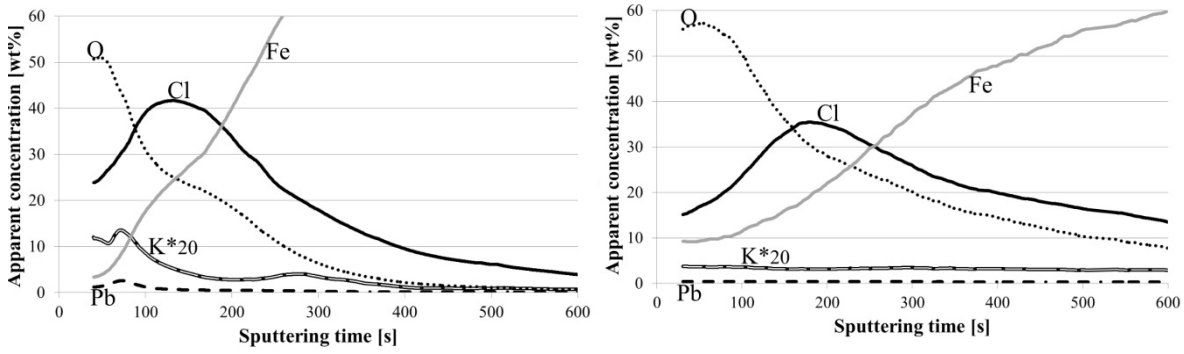

Figure 30.GD-OES depth profiles of 16Mo3 exposed to a) 100 % used-wood fuel and b) used-wood fuel + sewage sludge.

6.2.3 Stainless steels 310S

When the stainless steel 310S was exposed to 100 % used-wood fuel, corrosion occurred. Closest to the metal substrate, chlorine was present together with potassium, indicating the presence of potassium chloride. There were also areas where chlorine was not in obvious connection to potassium. Instead chromium was present in these areas, (see Figure 31), which indicates that chromium chloride is of importance for the corrosion process of stainless steels. Enrichments of nickel were observed in the alkali and metal chloride layer. The composition of these nickel rich areas indicates that the nickel was in metallic form and was a result of corrosion. A study by Jonsson et al. [50] reports on a similar behaviour and explains that the nickel originates from a nickel chloride that had transformed into iron and chromium chlorides due to its poor thermodynamic stability. Another explanation is that this nickel enrichment is the

result of the selective corrosion of chromium and iron, which resulted in a nickel-rich surface on the metal. This has also been suggested by other authors [8, 51].

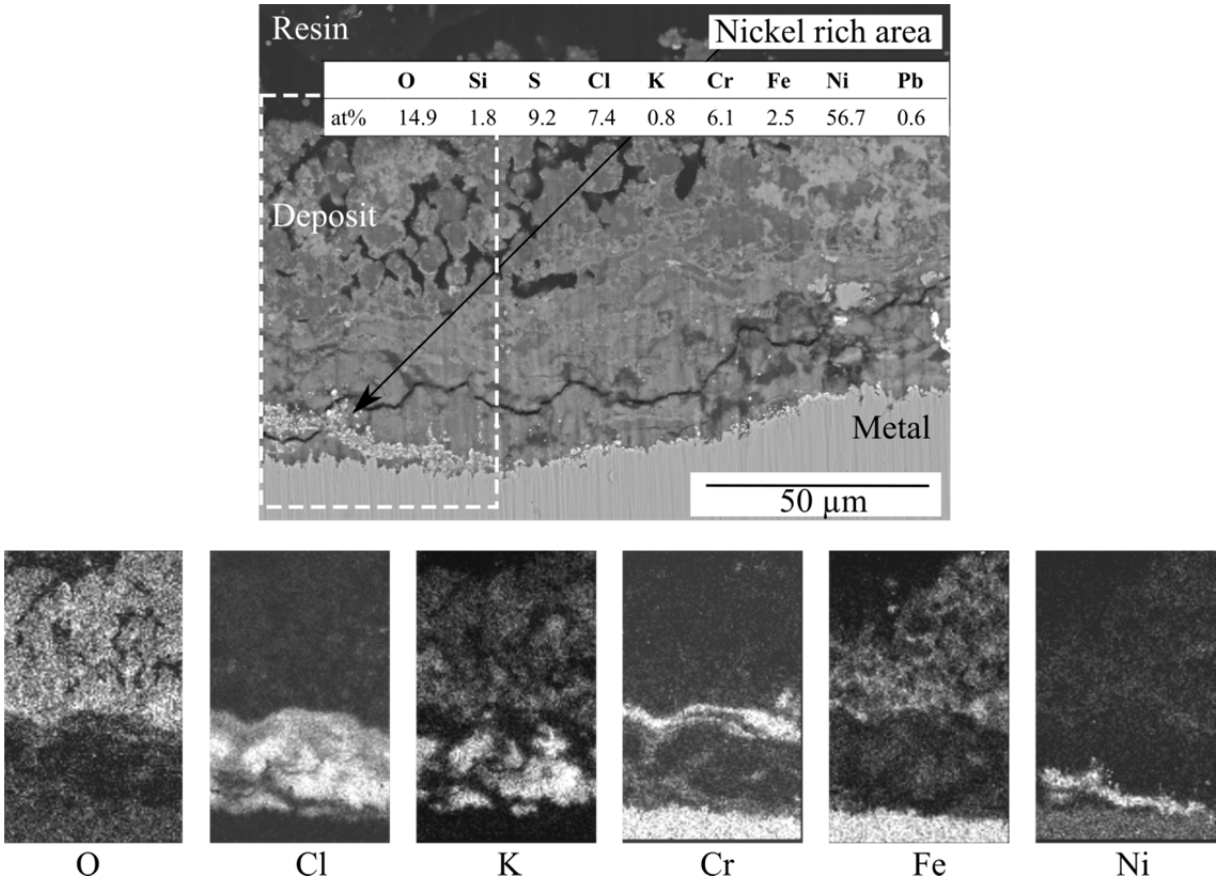

Figure 31. Cross section of 310S sample exposed to 100 % used-wood fuel at 350 °C showing nickel enrichment with EDS mapping and analysis point.

The nickel enrichment in the present study appeared to be particles that follow oxide growth and are not only located on the surface of the metal substrate. For this reason, the explanation with a nickel chloride origin is likely, but it is not possible to confirm which mechanism dominates based only on these results.

The chromium enrichment that was observed was not only connected to the chlorine, oxygen also overlapped to some extent, indicating a chromium oxide present below an area of iron enrichment. This layer-like structure can be seen above the chlorine-rich area (see Figure 31) and could originate in the formation of metal chlorides during the corrosion process. Assuming that iron, chromium and nickel all form metal chlorides in an initial step, a layer-like oxide structure will probably develop with time. The

reason for this is that the three metal chlorides have differences in volatility and thermodynamic stability. As discussed earlier, nickel probably transforms into iron and chromium chlorides. Both of these are volatile and can be assumed to evaporate through the oxide layer. The difference in thermodynamic stability at higher oxygen partial pressure will then result in a layered oxide structure with chromium oxide as the innermost layer since it more easily oxidises than iron chloride does. Similar behaviour has also been observed by other authors [8].

When sludge is added to the fuel a few features change that indicate that there is less corrosion when the additive is used. The nickel-enriched areas are no longer found in the cross section, the oxide layers are more uniform and iron does not migrate to the deposit in a manner similar to the sample exposed to 100 % used-wood fuel, (see Figure 32). Otherwise there are similarities to the sample exposed to 100% used-wood fuel with chlorine-rich areas close to the metal substrate sometimes partly overlapping with chromium, which indicates a similar initial corrosion process for this sample although slower.

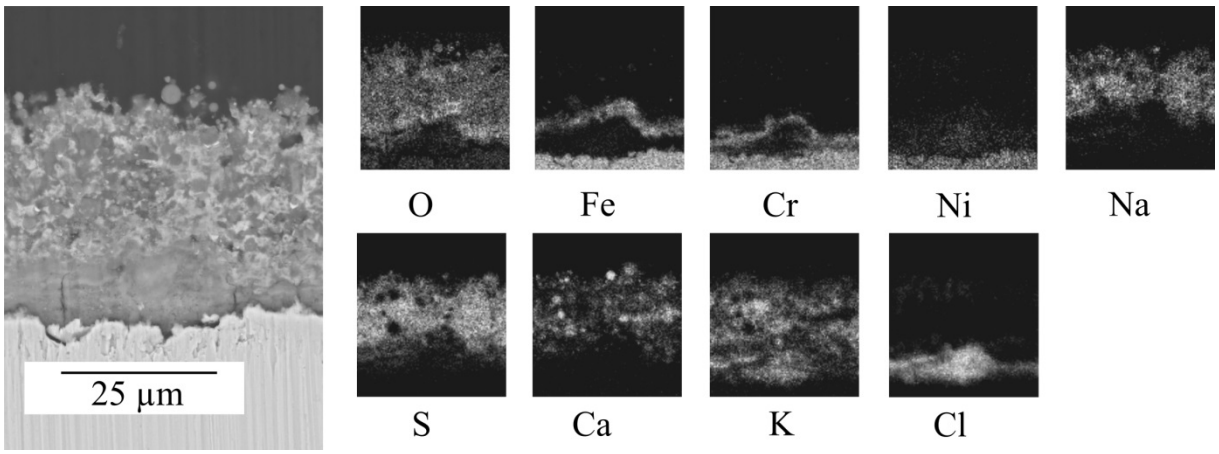

Figure 32. Cross section with elemental composition distribution of 310S exposed to used-wood fuel and sewage sludge addition at 350 °C.

6.2.4 Nickel-base alloy 625

Alloy 625 suffered from corrosion when exposed to 100 % used-wood fuel for 14 h at 400 °C in the field test. Nickel oxide can be seen mixed with the deposit, and a chromium enrichment can also be seen located close to this nickel oxide in Figure 33. The presence of nickel oxide was confirmed with XRD and SEM/EDS. With the use of XRD, lead potassium chromates were also found in the scraped-off deposit, which indicates that the initial corrosion of Alloy 625 is related to the formation of chromate, which dissolves the protective chromium oxide and leads to a less protective oxide. A high amount of chlorine was found close to the metal substrate, which further indicates that the protective chromia had been destroyed and opened the way for chlorine to reach the metal substrate.

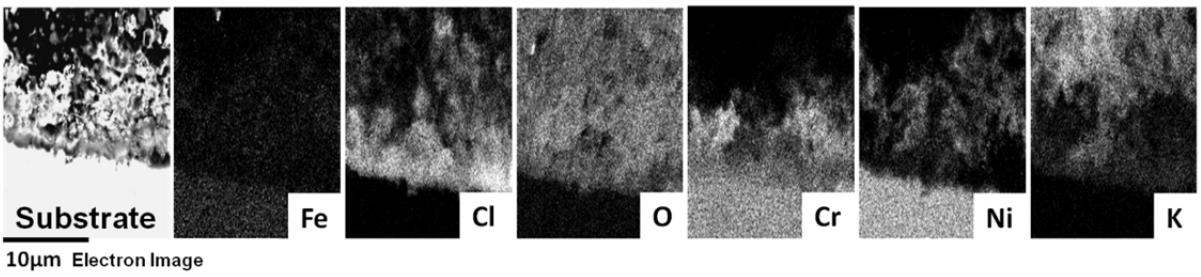

Figure 33. Cross section with elemental composition distribution of nickel base Alloy 625 exposed to used-wood at 400 °C.

When sewage sludge was co-fired with the used-wood fuel, the corrosion of Alloy 625 decreased. The nickel oxide and chromium-rich areas were not visible to the same extent as on the sample exposed to the fuel without the addition of sludge, (see Figure 34). Nevertheless, high amounts of potasssium and chlorine were found close to the metal substrate, which could possibly result in corrosion with time. No chromates were found with XRD, and the signal from chromium oxide was strong, indicating that a protective oxide is the reason for that less corrosion was observed.

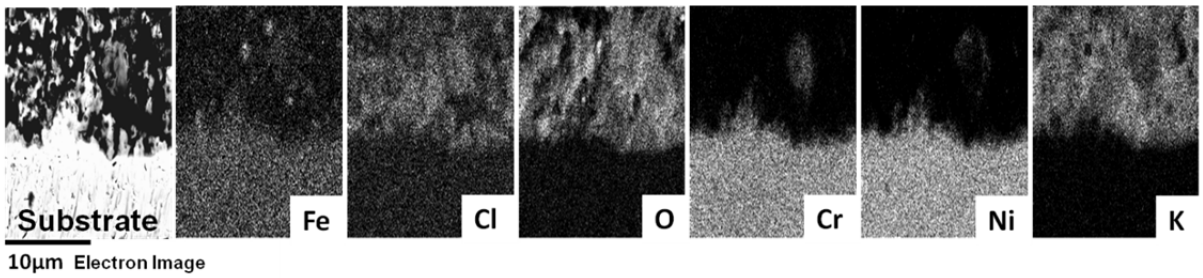

Figure 34. Cross section with elemental composition distribution of Alloy 625 exposed to used-wood fuel and sewage sludge addition at 400 °C.

6.2.5 Alumina-forming Kanthal APMT

Exposing the pre-oxidised Kanthal AMPT to the used-wood fuel resulted in corrosion of the alloy. It can be seen in Figure 35 that the alumina layer formed during pre-oxidation has dissolved, and the areas containing aluminium have become enriched in potassium. The compound $K_2Al_2O_4$ was found in the deposit and gives reason to believe that potassium chloride had reacted with the aluminium oxide (Paper I).

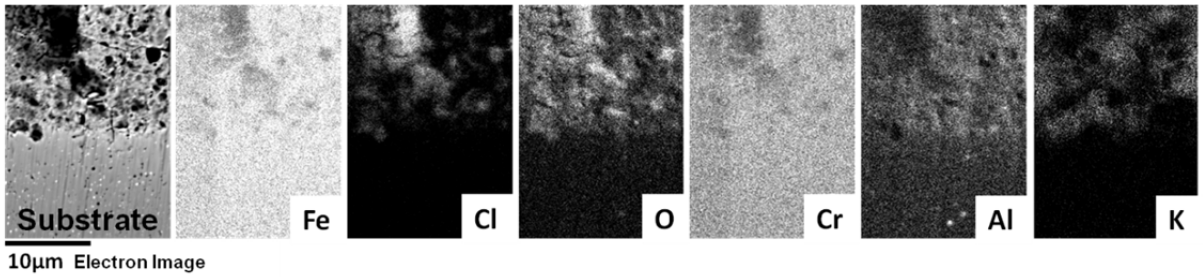

Figure 35. Cross section with elemental composition distribution of FeCrAl alloy Kanthal APMT exposed to used-wood fuel at 400 °C.

When sewage sludge is co-fired with used-wood fuel, the aluminium oxide is maintained on the sample, as shown in Figure 36. No potassium can be seen close to the oxide in the figure, and in the deposit, $K_2Al_2Si_2O_8$is present according to analysis with XRD (Table 9). The presence of this compound is not believed to be a result of corrosion. Instead this is believed to be a result of alumina silicates in the sewage sludge capturing potassium as predicted.

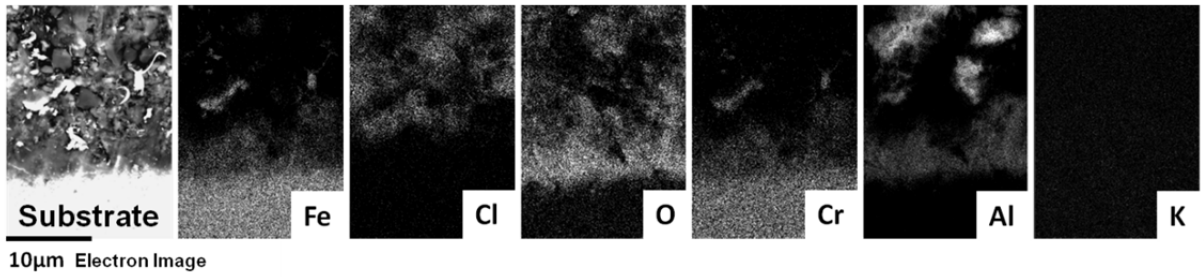

Figure 36. Cross section with elemental composition distribution of Alloy 625 exposed to used-wood fuel and sewage sludge addition at 400 °C.

The preservation of the aluminium oxide on the sample exposed to the used-wood fuel with a sludge addition and the absence of aluminium oxide on the sample exosed to the 100 % used-wood fuel was further demonstrated with depth profiling using GD-OES, (see Figure 37). For the samples exposed to used-wood fuel with sewage sludge addition, an aluminium oxide was observed at the metal interface. For the 100 % used-wood fuel sample, on the other hand, no aluminium enrichment was observed at the metal interface.

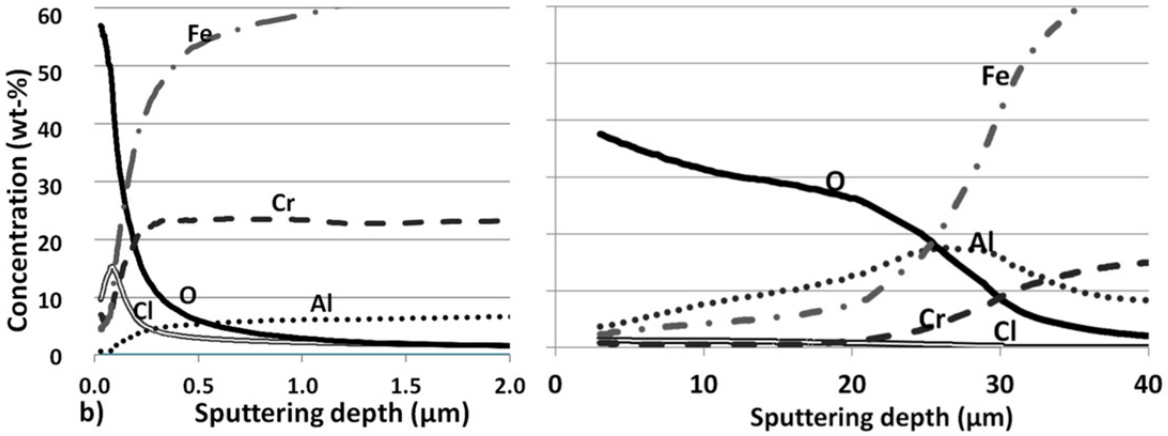

Figure 37. GD-OES depth profiles of Kanthal APMT exposed at 400 °C to a) 100 % used-wood fuel and b) used-wood + sewage sludge fuel.

6.3 Summary

The results in this thesis show that the corrosion of metallic materials exposed to used-wood fuels is a complex issue. A range of tested material types, consequently, results in variation in corrosion behaviour.

For the low-alloyed steel 16Mo3 the corrosion products observed throughout the study were iron chloride below an iron oxide layer. In some cases in which minor corrosion occurred, only the iron oxide was observed. Increasing the chromium and nickel content in the material, as for the stainless steel materials, introduced new elements that are supposed to improve the corrosion behaviour of the material. However, when this material type corroded it became clear that these species were also involved in the corrosion process. In the cases in which corrosion was observed on stainless steel, the general corrosion products seen were metal chlorides mixed with alkali chlorides closest to the metal substrate and metal oxides on top of this layer. In addition, particles rich in nickel were present close to the metal substrate. When the even higher alloyed nickel-base alloy 625 was exposed to used-wood fuel, this material also corroded. The corrosion resulted in nickel and chromium oxide formation or a migration of the species to the deposit. For this material, lead chromates were present as well in the scraped-off deposit/corrosion products. Figure 38 shows schematic illustrations of the typical corrosion products observed for the material types tested in the thesis when exposed to used-wood fuel. The alumina-forming Kanthal APMT was excluded from this illustration since it was pre-oxidised before exposure.

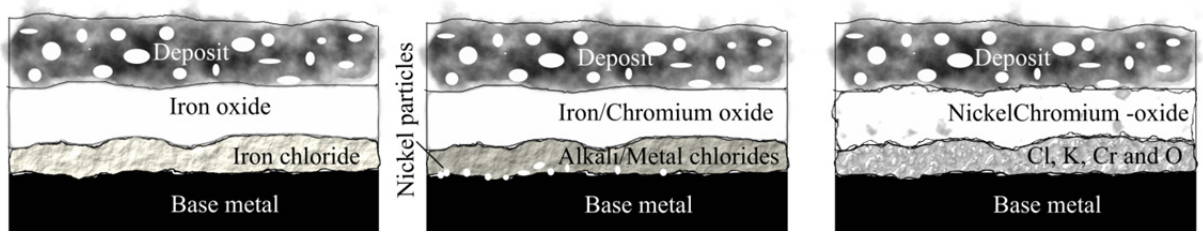

Figure 38. Schematic illustration of corrosion products commonly seen for three tested material groups exposed to used-wood fuel.

In general, the higher alloyed materials such as stainless steels (304L and 310S), nickel-base material (Alloy 625) and FeCrAl alloy Kanthal APMT showed better corrosion resistance when exposed to used-wood fuels than the 16Mo3 material. Also, these material groups showed less corrosion when municipal sewage sludge was co-fired with used-wood fuel.

An increase in lead content in the fuel clearly proved to have a negative effect on the corrosion behaviour of the low-alloyed steel 16Mo3. For the higher alloyed materials (304L and Alloy 625), no significant effect was observed. It is believed that the relatively short exposure time is one reason for this, and with longer exposure times, there is a risk that corrosion will occur also on these materials. In a study by Viklund et al. [1], lead-rich compounds were found close to the metal substrate in the deposit of a 304 alloy in combination with corrosion after 1550 h exposure at 500 °C. The increase in lead compounds close to the metal surface give reason to be concerned about an increase in the risk for the formation of chromate also on Alloy 625 since lead has been shown to be able to form chromates on nickel-base alloys [52].

Lead was frequently found to migrate towards the metal substrate. This suggests that studying a deposit composition from the surface in order to determine how corrosive a deposit is may not be sufficient. Instead cross sectioning and depth profiling with the use of GD-OES have shown to be useful options to study the location of lead compounds.

7 Conclusions

7.1 Effect of lead variation in used-wood fuels

An increase in lead concentration in a used-wood fuel affected the initial corrosion of the low-alloyed steel 16Mo3. At 350 °C, only minor corrosion was observed but an increase in corrosion with lead concentration in the fuel was indicated, which illustrates the corrosive effect of lead in a wood fuel. At 400 °C, the lead concentration greatly affected the corrosion rate of the low-alloyed steel 16Mo3. An additional corrosion process, besides chlorine-induced corrosion, where lead compounds are involved is proposed to be active. The iron chloride initially formed as a result of chlorine-induced corrosion is proposed to react with lead oxide and/or pure lead present in the deposit to form iron oxide and lead chloride. It was found that not only did the reaction between iron chloride and lead oxide/pure lead increase oxide growth, the lead chloride formation also resulted in the formation of low melting salt mixtures together with potassium chloride, traces of which were observed in the corrosion products.

For the higher alloyed materials, 304L and Alloy 625, the variation in lead concentration did not influence the corrosion mechanism in a way that resulted in a measurable corrosion attack in the test conditions and short exposure times that prevailed in this study.

7.2 Decreased corrosion with co-firing of municipal sewage sludge

In this study, it was found that the addition of municipal sewage sludge to a used-wood fuel decreased the corrosive elements present in the deposits on the materials exposed in the field test. The addition of municipal sewage sludge also decreased the initial corrosion for all the material groups tested. A minor effect was observed on the low-alloyed steel 16Mo3 material while the effect on the stainless steel 310S, the nickel-base alloy 625 and the pre-oxidised alumina-forming Kanthal APMT materials was greater. Several of the observed corrosion features were fewer with the addition of sewage sludge than when 100% used-wood fuel was used.

8 Acknowledgements

First of all, I want to thank my supervisors Jan-Erik Svensson and Rikard Norling for supporting me throughout this work and making it possible to work as an industrial PhD candidate in cooperation with Chalmers and Swerea KIMAB. The Swedish Energy Agency together with the High Temperature Corrosion Center (HTC) and KME - Consortium Materials Technology for thermal energy processes are acknowledged for their support and funding. I would also like to express my gratitude to Vattenfall, Valmet, E.ON, Outokumpu, Sandvik Materials Technology, Sandvik Heating Technology and Energiforsk for their contribution to the projects.

I want to give an extra warm acknowledgment to Rikard Norling! His support through this work has been very important and meant much to me!

I also want to thank my co-authors Yousef Alipour, Pamela Henderson, Anders Hjörnhede and Leyla Wickström for contributing to the thesis. I have enjoyed working with you, and I hope we will meet in projects also in the future.

Special thanks to Fredrik Lindberg and Haiping Lai for assistance with performing FIB cross sections. Arne Bengtsson and Mats Randelius are acknowledged for performing GD-OES analysis and providing expertise during the evaluation of results.

Mattias Mattson at Vattenfall and Fredrik Niklasson at SP are acknowledged for their valuable work during the field and laboratory exposures together with Anna Helgesson, Carl Nordenskjöld, Daniel Ryde and Annika Stålenheim.

This work would not have been possible without the support from my employee, Swerea KIMAB, thank you! All my co-workers at Swerea KIMAB are greatly acknowledged for contributing to a pleasant working environment!

Least, but opposite to last, my family, I love you!

Paul and William, you fill my life with joy and happiness! I want to direct an extra important acknowledgment to you Paul for always helping and encouraging me.

9 References

[1] P. Viklund, A. Hjörnhede, P. Henderson, A. Stålenheim, and R. Pettersson, *"Corrosion of superheater materials in a waste-to-energy plant," Fuel Processing Technology*", 2013, 105, pp.106-112.

[2] Y. Alipour and P. Henderson, *"Corrosion of furnace wall materials in waste-wood fired power plant",* Corrosion Engineering, Science and Technology, 2015, 50, pp. 355-363

[3] N. Folkeson, L. G. Johansson, and J. E. Svensson, *"Initial stages of the HCl-induced high-temperature corrosion of Alloy 310"* Journal of Electrochemical Society, 2007, 154, pp. C515-C521

[4] H. Asteman and M. Spiegel, *"Investigation of the HCl (g) attack on pre-oxidized pure Fe, Cr, Ni and commercial 304 steel at 400°C"* Corrosion Science, 2007, 49, pp. 3626-3637.

[5] J. Pettersson, J. E. Svensson, and L. G. Johansson, *"KCl-induced corrosion of a 304-type austenitic stainless steel in O_2 and in O_2 + H_2O environment: The influence of temperature,"* Oxidation of Metals, 2009, 72, pp. 159-177.

[6] J. Lehmusto, P. Yrjas, B. J. Skrifvars, and M. Hupa, *"High temperature corrosion of superheater steels by KCl and K_2CO_3 under dry and wet conditions",* Fuel Processing Technology, 2012, 104, pp. 253-264.

[7] S. Karlsson, J. Pettersson, J. E. Svensson, and L. G. Johansson, *"KCl-induced high temperature corrosion of the austenitic stainless steel 304L; - the influence of SO_2*", Materials Science Forum, 2011, 696, pp. 224-229.

[8] S. Enestam, D. Bankiewicz, J. Tuiremo, K. Mäkelä, and M. Hupa, *"Are NaCl and KCl equally corrosive on superheater materials of steam boilers?",* Fuel, 2013, 104, pp. 294-306.

[9] B. Strömberg and S. Svärd Herstad, *"The Fuel Handbook 2012",* Stockholm, Värmeforsk 2012.

[10] J. Krook, A. Mårtensson, and M. Eklund, *"Sources of heavy metal contamination in Swedish wood waste used for combustion"* Waste Management, 2006, vol. 26, pp. 158-166.

[11] J. Krook, A. Mårtensson, and M. Eklund, *"Metal contamination in recovered waste wood used as energy source in Sweden,"* Resources, Conservation and Recycling, 2004, vol. 41, pp. 1-14.

[12] S. Enestam, C. Boman, J. Niemi, D. Boström, R. Backman, K. Mäkelä, et al., *"Occurrence of Zinc and Lead in Aerosols and Deposits in the Fluidized-Bed Combustion of Recovered Waste Wood. Part 1: Samples from Boiler,"* Energy & Fuels, 2011, 25, pp. 1396-1404.

[13] A. Talus, R. Norling, and P. Henderson, *"Influence of ammonium sulphate additive on superheater corrosion at increased steam temperature during combustion of recycled wood",* presented at the 10th Liège Conference on Materials for Advanced Power Engineering, Liege, 2014.

[14] M. Broström, H. Kassman, A. Helgesson, M. Berg, C. Andersson, R. Backman, et al., *"Sulfation of corrosive alkali chlorides by ammonium sulfate in a biomass fired CFB boiler,"* Fuel Processing Technology, 2007, 88, pp. 1171-1177.

[15] P. Viklund, R. Petterson, A. Hjörnhede, P. Henderson, and P. Sjövall, *"Effect of sulphur containing additive on initial corrosion of superheater tubes in waste fired boiler",* Corrosion Engineering, Science and Technology, 2009, 44, pp. 234-240.

[16] H. Kassman, J. Pettersson, B.-M. Steenari, and L.-E. Åmand, *"Two strategies to reduce gaseous KCl and chlorine in deposits during biomass combustion — injection of ammonium sulphate and co-combustion with peat",* Fuel Processing Technology, 2013, 105, pp. 170-180.

[17] A.-S. Khanna, *"Introduction to High Temperature Oxidation and Corrosion"*, 2002, Ohio, USA: ASM International.

[18] N. Birks, G. H. Meier, and F. S. Pettit, *"Introduction to the High Temperature Oxidation of Metals"* 2006, Cambridge: Cambridge University Press.

.

[19] P. Kofstad, "High Temperature Corrosion", 1988, London, UK: Elsevier Applied Science.

[20] L. Wester, "Förbränningsteknik", 1991, Västerås.

[21] S. V. Vassilev, D. Baxter, L. K. Andersen, and C. G. Vassileva, *"An overview of the chemical composition of biomass",* Fuel, 2010, 89, pp. 913-933.

[22] S. Enestam, K. Mäkelä, R. Backman, and M. Hupa, *"Occurrence of Zinc and Lead in Aerosols and Deposits in the Fluidized-Bed Combustion of Recovered Waste Wood. Part 2: Thermodynamic Considerations",* Energy & Fuels, 2011, 25, pp. 1970-1977.

[23] S. Enestam, R. Backman, K. Mäkelä, and M. Hupa, *"Evaluation of the condensation behavior of lead and zinc in BFB combustion of recovered waste wood",* Fuel Processing Technology, 2013, 105, pp. 161-169.

[24] M. Broström, S. Enestam, R. Backman, and K. Mäkelä, *"Condensation in the KCl-NaCl system",* Fuel Processing Technology, 2013, 105, pp. 142-148.

[25] Y. Alipour, P. Henderson, and P. Szakálos, *"The effect of a nickel alloy coating on the corrosion of furnace wall tubes in a waste wood fired power plant",* Materials and Corrosion, 2014, 65, pp. 217-225.

[26] H. J. Grabke, E. Reese, and M. Spiegel, *"The effects of chlorides, hydrogen chloride, and sulfur dioxide in the oxidation of steels below deposits",* Corrosion Science, 1995, 37, pp. 1023-1043.

[27] P. Henderson, P. Szakálos, R. Pettersson, C. Andersson, and J. Högberg, *"Reducing superheater corrosion in wood-fired boilers",* Materials and Corrosion, 2006. 57, pp. 128-134.

[28] H. Asteman, J. E. Svensson, L. G. Johansson, and M. Norell, *"Indication of chromium oxide hydroxide evaporation during oxidation of 304L at 873 K in the presence of 10% water vapor",* Oxidation of Metals, 1999, 52, pp. 95-111.

[29] J. Pettersson, H. Asteman, J. E. Svensson, and L. G. Johansson, *"KCl induced corrosion of a 304-type austenitic stainless steel at 600°C; the role of potassium",* Oxidation of Metals, 2005, vol. 64, pp. 23-41.

[30] J. Pettersson, N. Folkeson, L.-G. Johansson, and J.-E. Svensson, *"The Effects of KCl, K2SO4 and K2CO3 on the High Temperature Corrosion of a 304-Type Austenitic Stainless Steel",* Oxidation of Metals, 2011, 76, pp. 93-109.

[31] N. Folkeson, T. Jonsson, M. Halvarsson, L. G. Johansson, and J. E. Svensson, *"The influence of small amounts of KCl(s) on the high temperature corrosion of a Fe-2.25Cr-1Mo steel at 400 and 500°C",* Materials and Corrosion, 2011, 62, pp. 606-615.

[32] I. Barin, *"Thermochemical data of pure substances",* 1995, Weinheim, Germany: VCH

[33] M. Levin, *"Phase diagrams for Ceramists,"* 1969, Ohio, USA, The American ceramic Society.

[34] A. Ruh and M. Spiegel, *"Thermodynamic and kinetic consideration on the corrosion of Fe, Ni and Cr beneath a molten KCl–$ZnCl_2$ mixture", 2006,* Corrosion Science, 48, pp. 679-695.

[35] M. Spiegel, *"Salt melt induced corrosion of metallic materials in waste incineration plants",* Materials and Corrosion, 1999, 50, pp. 373-393.

[36] D. Bankiewicz, S. Enestam, P. Yrjas, and M. Hupa, *"Experimental studies of Zn and Pb induced high temperature corrosion of two commercial boiler steels",* Fuel Processing Technology, 2013, 105, pp. 89-97.

[37] A. Ruh and M. Spiegel, *"Kinetic investigations on salt melt induced high-temperature corrosion of pure metals"* in Materials Science Forum 2004, 461-464, pp. 61-68.

[38] B. J. Skrifvars, R. Backman, M. Hupa, K. Salmenoja, and E. Vakkilainen, *"Corrosion of superheater steel materials under alkali salt deposits Part 1: The effect of salt deposit composition and temperature"* Corrosion Science, 2008, 50, pp. 1274-1282.

[39] M. Aho, *"Reduction of chlorine deposition in FB boilers with aluminium-containing additives",* Fuel, 2001, 80, pp. 1943-1951.

[40] M. Aho, P. Yrjas, R. Taipale, M. Hupa, and J. Silvennoinen, *"Reduction of superheater corrosion by co-firing risky biomass with sewage sludge"* Fuel, 2010, 89, pp. 2376-2386.

[41] L. Amand, B. Leckner, D. Eskilsson, and C. Tullin, *"Deposits on heat transfer tubes during co-combustion of biofuels and sewage sludge",* Fuel, 2006, 85, pp. 1313-1322.

[42] A. Elled, L. Amand, B. Leckner, and B. Andersson, *"Influence of phosphorus on sulphur capture during co-firing of sewage sludge with wood or bark in a fluidised bed",* Fuel, 2006, 85, pp. 1671-1678.

[43] T. Jonsson, J. Petterson, K. Davidsson, L. G. Johansosn, and J.-E. Svensson, *"Sewage sludge as additive to reduce the initial fireside corrosion caused by combustion of shredder residues in a waste-fired BFB boiler,"* presented at the 9th Liège Conference on Materials for Advanced Power Engineering, Liege, 2010.

[44] S. Karlsson, L. E. Åmand, and J. Liske, *"Reducing high-temperature corrosion on high-alloyed stainless steel superheaters by co-combustion of municipal sewage sludge in a fluidised bed boiler",* Fuel, 2015, 139, pp. 482-493.

[45] P. J. Goodhew, J. Humphreys, and R. Beanland, *Electron Microscopy and Analysis, Third Edition:* London: Taylor & Francis, 2000.

[46] R. Jenkins and R. Snyder, *"Introduction to X-Ray Powder Diffractometry",* New York: Wiley, 2012.

[47] Y. Alipour, P. Henderson, and P. Szakalos, "*Effect of temperature on corrosion of furnace walls in a waste wood fired boiler",* Materials at High Temperatures, 2015, 32, pp. 188-196.

[48] I. P. Parkin and A. T. Rowley, *"Metathesis routes to tin and lead chalcogenides",* Polyhedron, 1993, 12, pp. 2961-2964.

[49] A. F. Scott, *"Survey of Progress in Chemistry",* 1964, New York: Academic Press.

[50] T. Jonsson, N. Folkeson, M. Halvarsson, J. E. Svensson, and L. G. Johansson, *"Microstructural investigation of the hcl-induced corrosion of the austenitic alloy 310S (52Fe26Cr19Ni) at 500°C",* Oxidation of Metals, 2014, 81, pp. 575-596.

[51] S. C. Van Lith, F. J. Frandsen, M. Montgomery, T. Vilhelmsen, and S. A. Jensen, *"Lab-scale investigation of deposit-induced chlorine corrosion of superheater materials under simulated biomass-firing conditions. Part 1: Exposure at 560°C",* Energy and Fuels, 2009, 23, pp. 3457-3468.

[52] D. Chatterji, D. W. McKee, G. Romeo, and H. S. Spacil, *"The Effects of Lead on the Hot Corrosion of Nickel-Base Alloys",* Journal of the Electrochemical Society, 1975, 122, pp. 941-952.